

METALLURGICAL INVESTIGATION OF
CRACKING IN A REACTOR VESSEL NOZZLE SAFE-END

SWRI PROJECT 02-5389-001

INTERIM REPORT

To

Iowa Electric Power
Cedar Rapids

October 20

Prepared by:

H. C. Burghard, Jr.

— NOTICE —

THE ATTACHED FILES ARE OFFICIAL RECORDS OF THE DIVISION OF DOCUMENT CONTROL. THEY HAVE BEEN CHARGED TO YOU FOR A LIMITED TIME PERIOD AND MUST BE RETURNED TO THE RECORDS FACILITY BRANCH 016. PLEASE DO NOT SEND DOCUMENTS CHARGED OUT THROUGH THE MAIL. REMOVAL OF ANY PAGE(S) FROM DOCUMENT FOR REPRODUCTION MUST BE REFERRED TO FILE PERSONNEL.

DEADLINE RETURN DATE

50-331

RETURN TO REGULATORY GENERAL FILES
ROOM 016

Bucket # 50-331

Control # 7810310220

DATE 10/27/78

REGULATORY BRANCH

RECORDS FACILITY BRANCH

for Clifford H. Wells
U. S. Lindholm, Director
Department of Materials Sciences

781031 0227

TABLE OF CONTENTS

	<u>PAGE</u>
1.0 INTRODUCTION	1
2.0 MACROSCOPIC ASPECTS OF CRACKING	6
2.1 Nondestructive Inspections	6
2.2 Crack Location and Configuration	6
3.0 MATERIALS CHARACTERIZATION	13
3.1 Chemical Composition	13
3.2 Microstructure	13
4.0 CHARACTERIZATION OF CRACKING	23
4.1 Microstructural Features	23
4.2 Fractographic Features	24
5.0 SURFACE DEPOSIT ANALYSES	38
6.0 SUMMARY AND CONCLUSIONS	39
APPENDIX A - Radiographs	A-1
APPENDIX B - Macrographs of Metallographic Sections	B-1

1.0 INTRODUCTION

A safe-end forging, removed from a recirculation inlet nozzle of the reactor vessel at the Duane Arnold Energy Center was submitted to SwRI by Iowa Electric Light and Power Company. A diagram of the recirculation inlet nozzle with the attached safe-end and thermal sleeve is shown in Figure 1-1. The safe-end sample, shown in Figure 1-2, was identified as recirculation unit nozzle 2A. Through-wall cracking had developed in service over approximately 85° of the outside circumference (from 75° clockwise to 160°). The appearance of the crack on the outside surface is shown in Figure 1-3. A metallurgical examination of the safe-end was initiated to establish the nature and extent of cracking and to identify the mechanism and cause of failure. This report is submitted to present the data and information obtained to date in the investigation.

The safe-end sample has been cut to provide the various metallurgical sections and samples shown in Figure 1-4. All saw cutting operations were performed dry to prevent contamination of the samples. The tests and examinations performed to date have included an ultrasonic inspection of the safe-end, chemical analyses of safe-end and thermal sleeve materials, metallographic examination of three representative sections through the thermal sleeve attachment area and microhardness measurements at selected locations. Fractographic examination of two representative crack surface specimens, and analyses of surface deposits have also been performed.

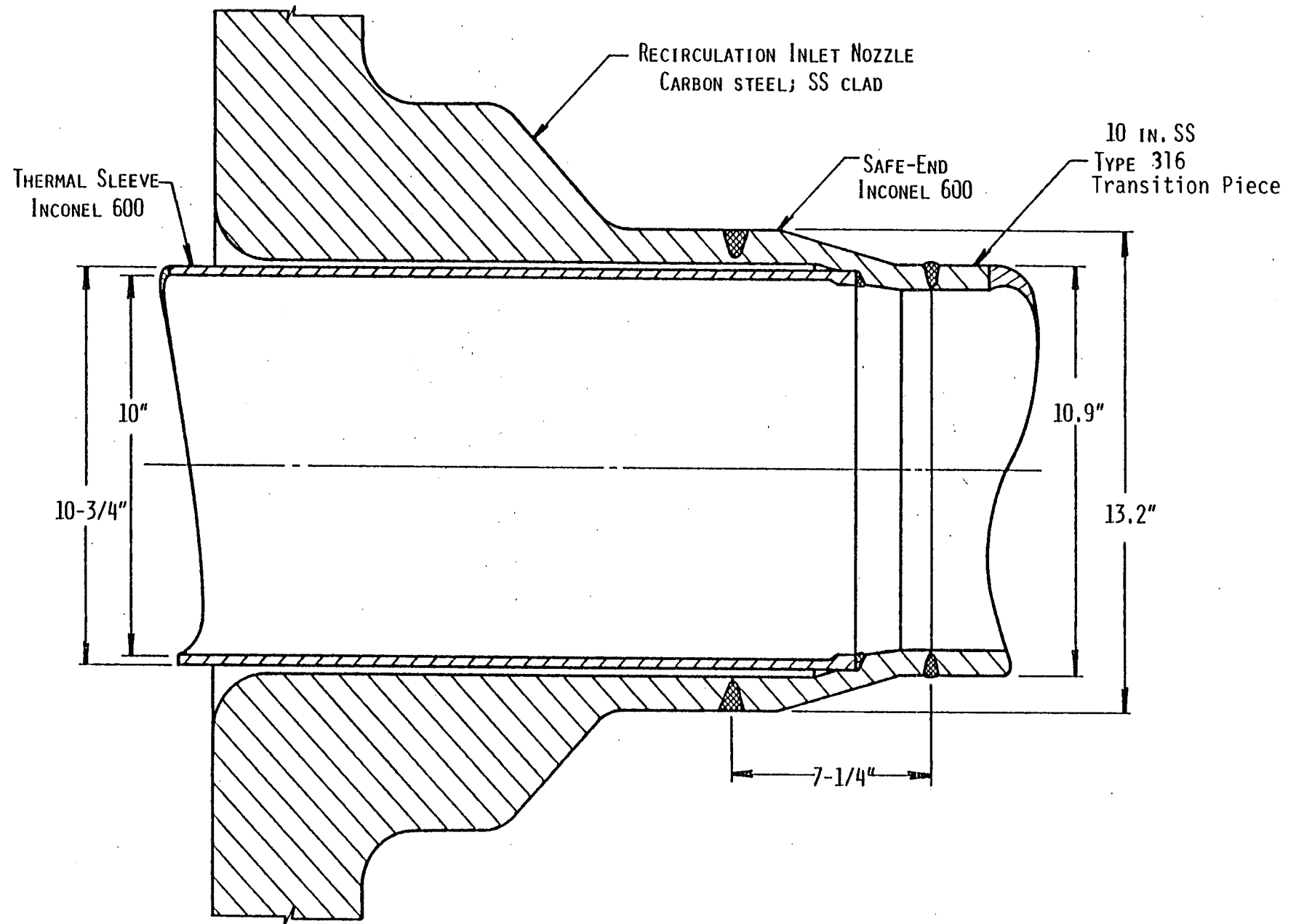
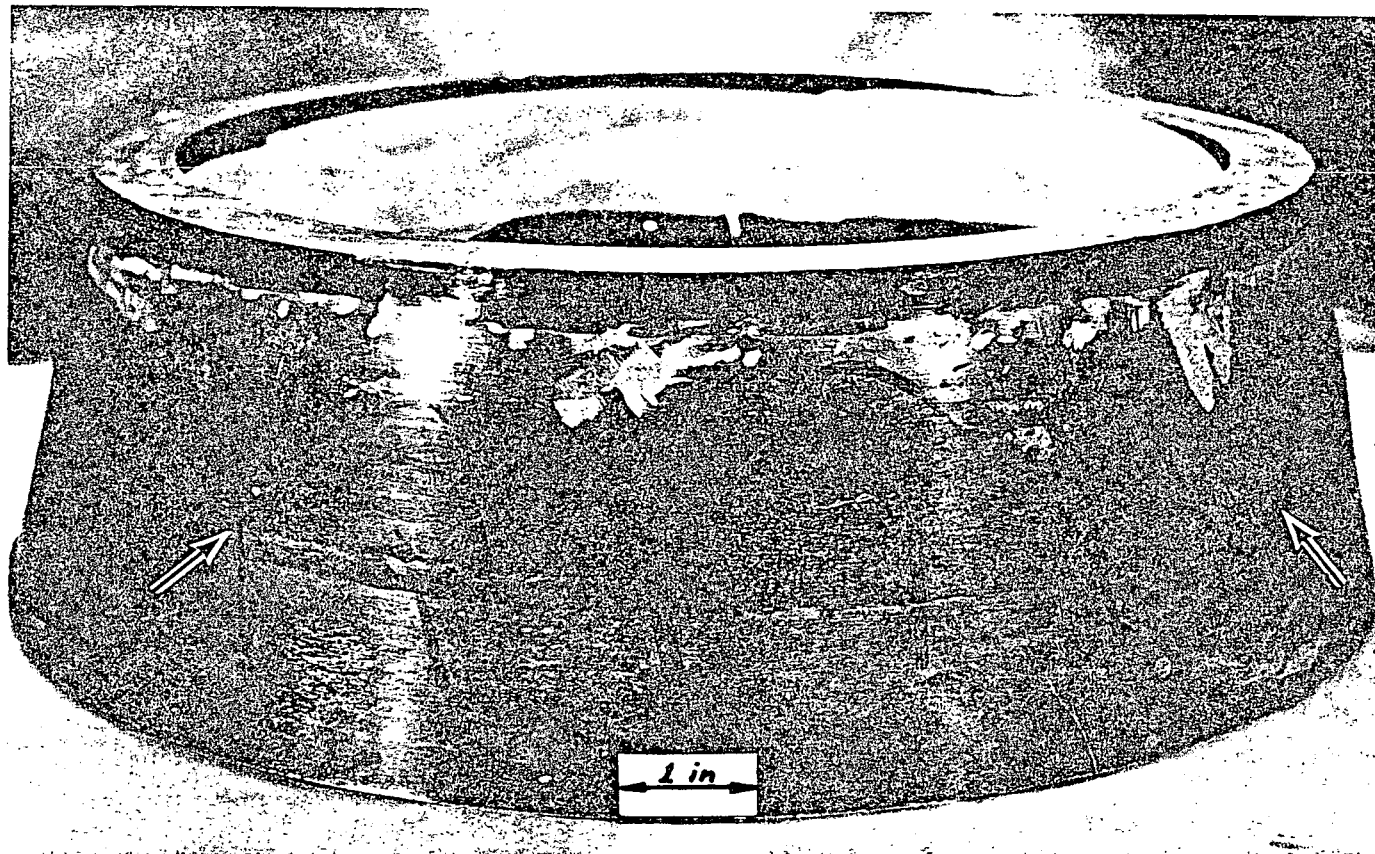
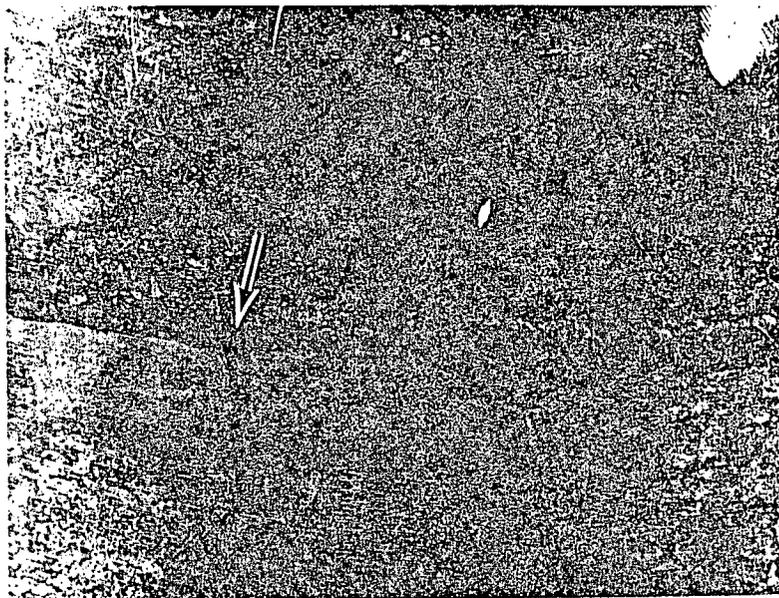


FIGURE 1-1. RECIRCULATION INLET NOZZLE



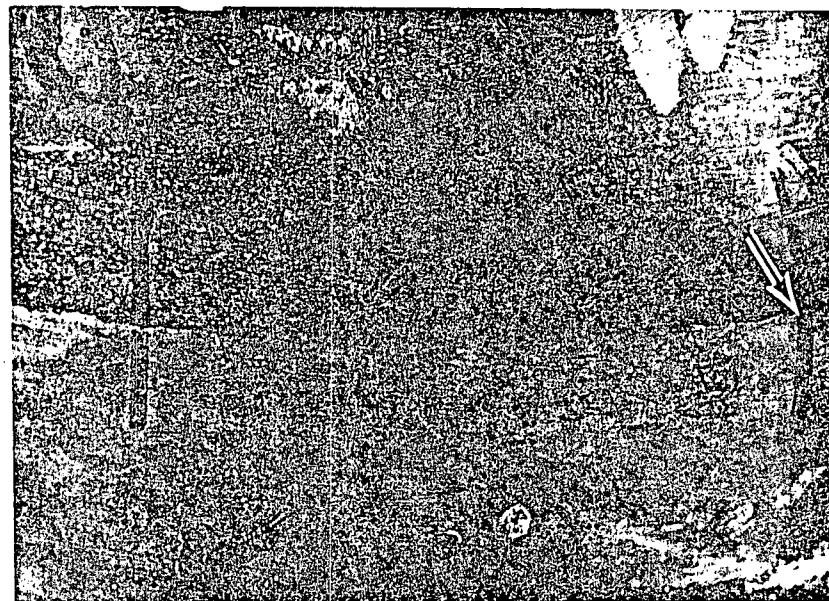
2-34314

FIGURE 1-2. SAFE-END SAMPLE. Arrows mark the ends of the through-wall-crack.



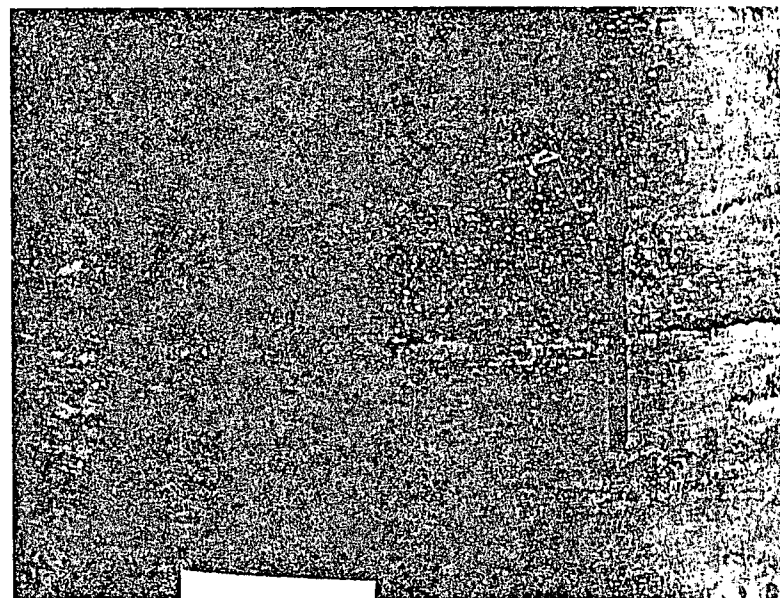
2-34320

(a) At 150°



2-34322

(b) At 90°



2-34321

(c)

FIGURE 1-3. CRACK ON OUTSIDE SURFACE OF SAFE-END.
Arrows indicate end of through-wall crack.
Note shift in crack path in (c). Actual size.

2.0 MACROSCOPIC ASPECTS OF CRACKING

2.1 Nondestructive Inspections

A radiographic inspection of the safe-end was performed on site at the Duane Arnold Energy Center after removal of the safe-end sample from the reactor vessel. This inspection identified major cracking over approximately 280° of the circumference. No identifiable crack indications were noted in the segment extending from 270° to 345° . Copies of representative portions of the radiographs are included in Appendix A.

A limited ultrasonic inspection of the safe-end sample was performed after receipt at SwRI. A 1.5 MHz transducer was employed in the inspection and the sound beam was directed from the large end toward the smaller end. The cracking in the safe-end was readily detectable by this technique. Particular attention was paid to the zone in which no definite radiographic crack indications were obtained. Definite ultrasonic crack indications were noted over the entire segment from 270° to 0° , establishing that major cracking extended completely around the inside surface of the safe-end.

2.2 Crack Locations and Configuration

A total of 11 longitudinal sections were examined macroscopically to establish the general location and configuration of cracking. As shown in Figure 1-4, the particular sections included locations near each end of the through-wall portion of the crack and sections selected on the basis of the radiographic crack indications to provide for evaluation over the complete circumference.

A diagram of a typical longitudinal section, showing the relative positions of the attachment weld, crevice, and repair weld is shown in Figure 2-1. Macrographs of representative sections are shown in Figures 2-2, 2-3, and 2-4. Additional macrographs are included in Appendix B.

Significant cracking was evident in all of the sections examined. At all locations, the crack originated in the general area of the tip of the crevice adjacent to the attachment weld and extended outward through the safe-end wall. In that portion of the through-wall crack extending from approximately 125° to 160° , the later stages of cracking

propagated through the repair weld, see Figures 2-2 and B-1 and Figure 1-3(a). In the zone from approximately 75° to 125° crack propagation occurred completely within the safe-end base metal and penetrated the outside surface adjacent to the fusion line of the repair weld, see Figures 2-3 and 1-3(b).

The crack length and remaining ligament (radial distance from the crack tip to the outside surface) were measured in all 11 sections. The results are plotted in Figure 2-5. Examination of sections 5-5, 8-8, 9-9, 10-10 and 11-11 verified the existence of major cracking in the zone from 270° to 330° . The radiographic inspection of this area did not reveal definite crack indications.

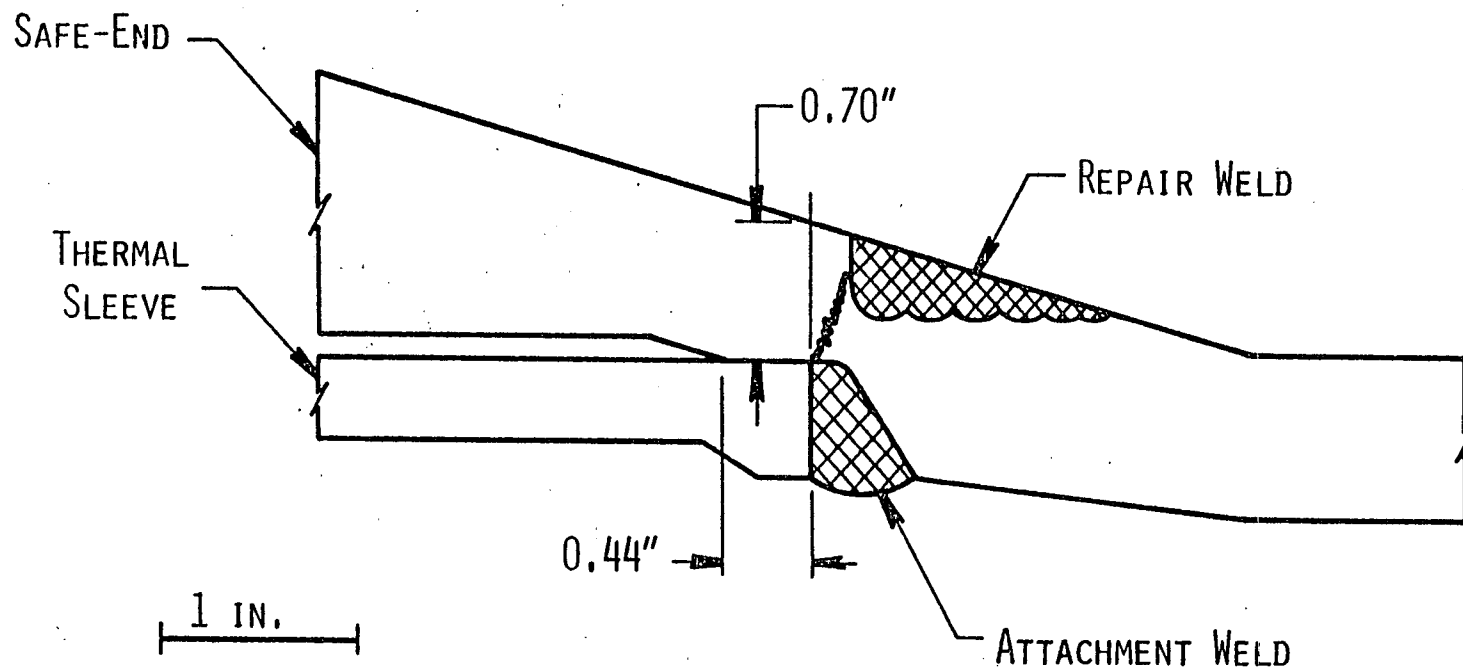
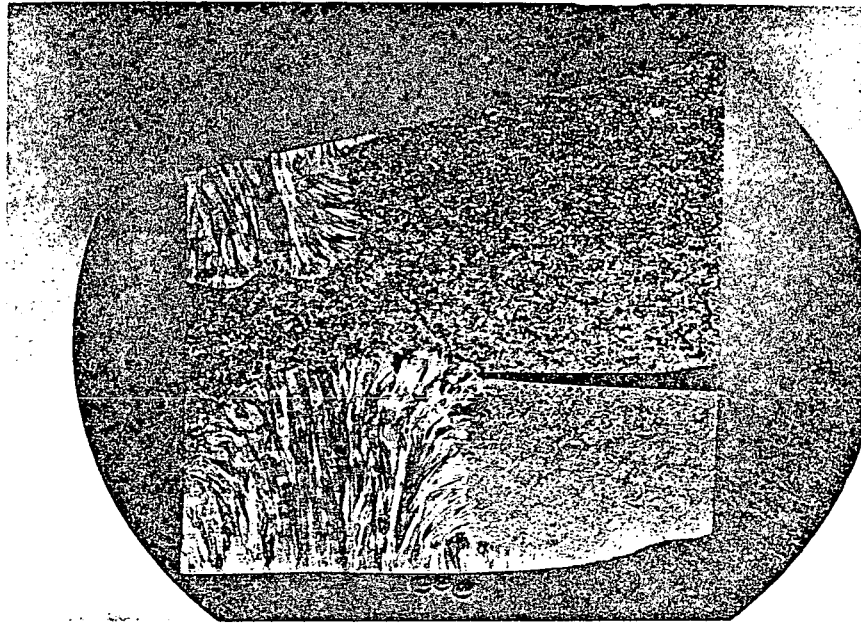
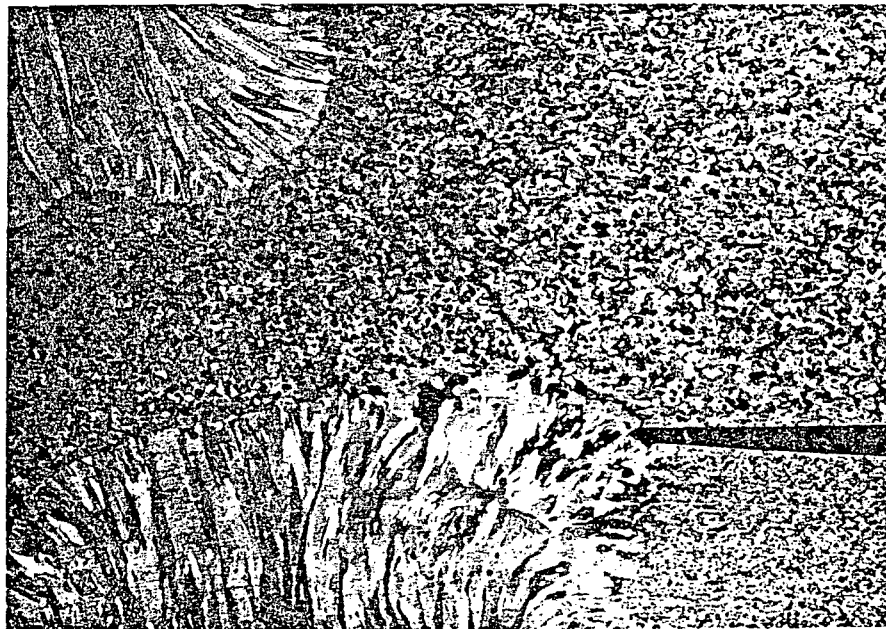


FIGURE 2-1. TYPICAL LONGITUDINAL SECTION THROUGH THERMAL SLEEVE ATTACHMENT AREA



2-34348

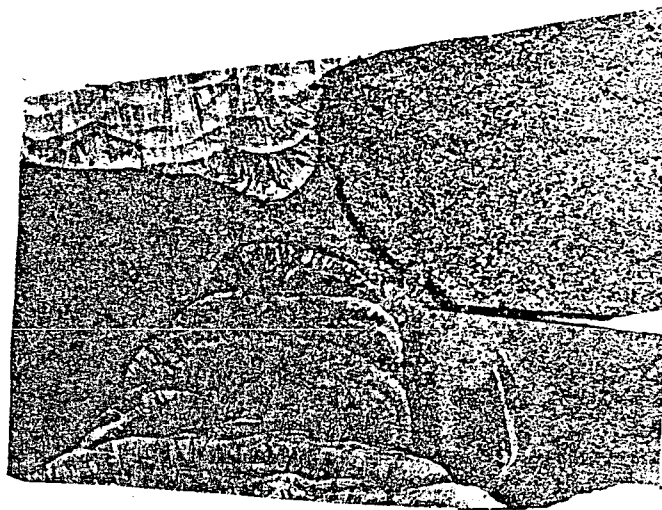
2X



2-34349

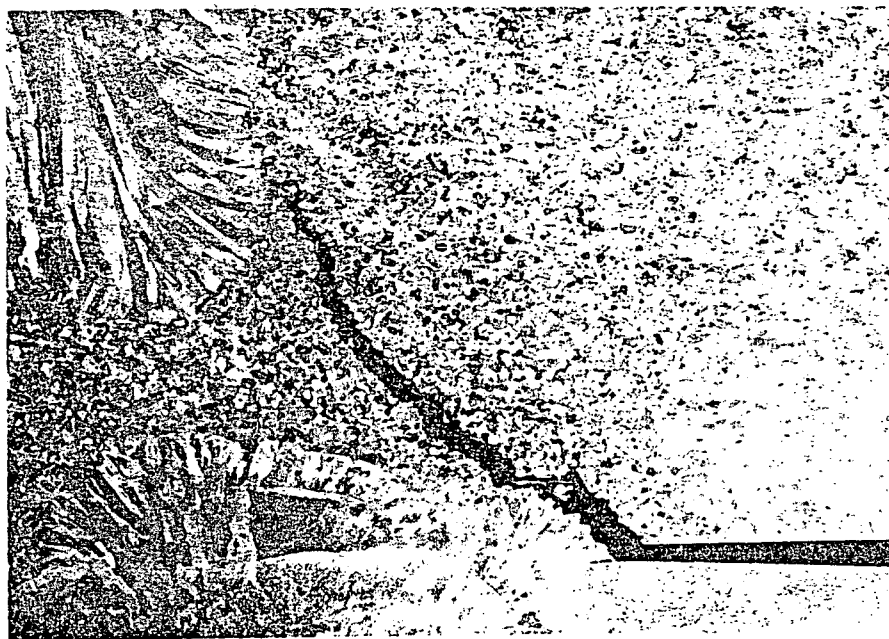
5X

FIGURE 2-2. LONGITUDINAL SECTION AT THERMAL SLEEVE ATTACHMENT.
Section 1-1, Figure 1-4. Lapito's etch.



2-34461

2X



2-34462

5X

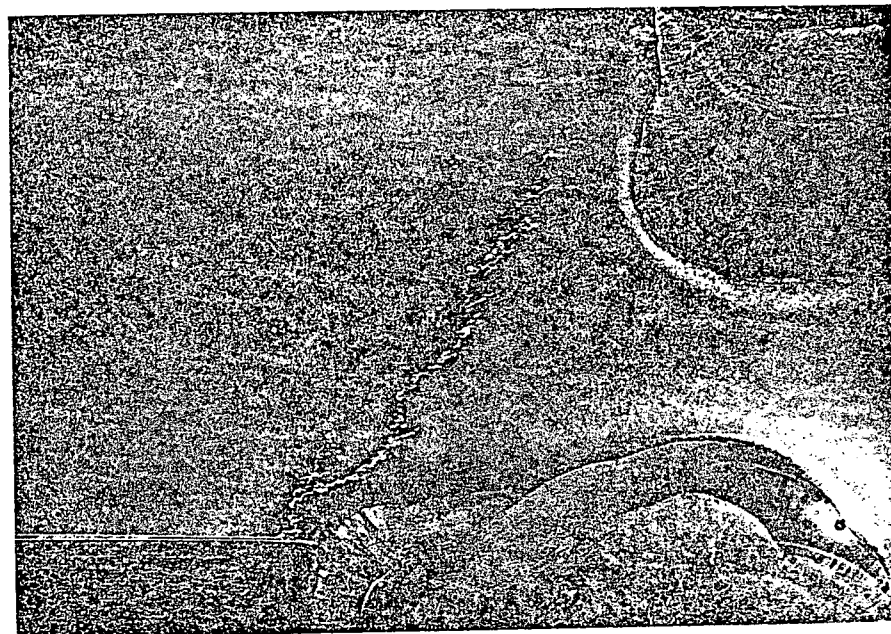
FIGURE 2-3. LONGITUDINAL SECTION AT THERMAL SLEEVE ATTACHMENT.
Section 4-4, Figure 1-4. Lapito's etch.



2-34447

Lapito's etch

2X



2-34492

Etchant: 8:1
Phosphoric acid

5X

FIGURE 2-4. LONGITUDINAL SECTION AT THERMAL SLEEVE ATTACHMENT.
Section 5-5, Figure 1-4.

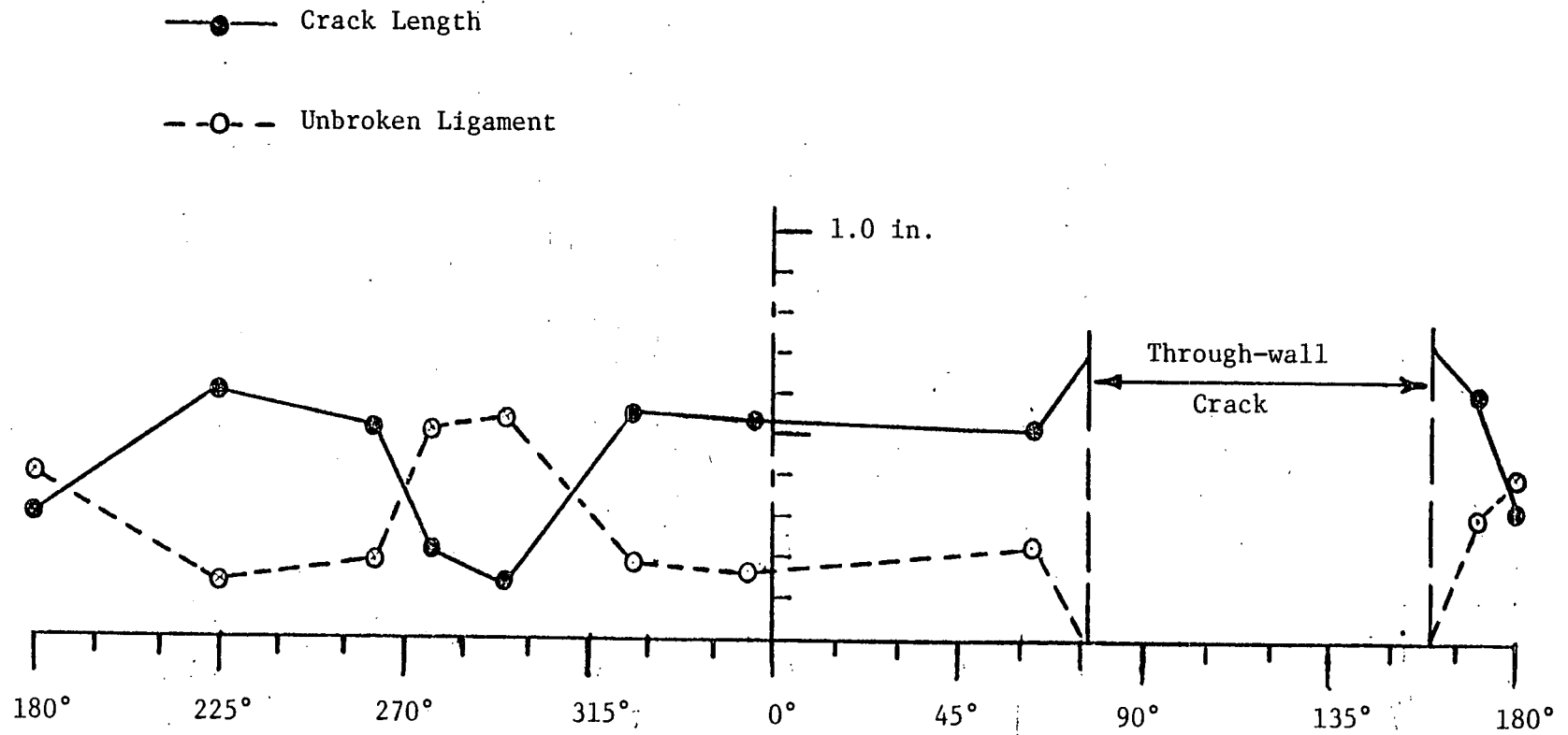


FIGURE 2-5. CRACK LENGTH AND UNBROKEN LIGAMENT VS ANGULAR POSITION

3.0 MATERIALS CHARACTERIZATION

3.1 Chemical Composition

Samples of the safe-end, thermal sleeve, attachment weld metal and repair weld metal were analyzed to determine the bulk chemical composition. The results of these analyses are presented in Table 3-1 together with the composition limits specified by ASME SB 166 for wrought Inconel 600 and by AWS-5.11-76.

These analyses established that both the safe-end forging and the thermal sleeve material conform to the compositional requirements of SB 166. It was reported that Inconel 182 stick electrodes were employed for the weld repair and thermal sleeve attachment weld. The compositions of both weld deposits conform to the specified compositions for deposited ENiCrFe-3 weld deposit metal (Inconel 182).

3.2 Microstructure

The typical microstructure of the safe-end forging, as observed at locations remote from the welds, is shown in Figure 3-1. The micrographs shown illustrate the microstructural features revealed by dual etching. The specimens were polished and etched in 10% nital and examined on the optical metallograph. Subsequently, the specimens were repolished, reetched in 8:1 phosphoric acid, and examined at the identical location to provide a direct comparison of microstructural features revealed by the two etching techniques.

The 10% nital etch will delineate grain boundaries in Inconel 600 regardless of the heat treating condition. The phosphoric acid etch selectively attacks precipitated carbides in the microstructure. As a result, grain boundaries and other microstructural features are delineated by this etch only if they are decorated with precipitated carbides. Thus, the lack of any grain boundary etching effect with the phosphoric acid etch, at a location where grain boundaries have been identified by a nital etch, is a specific indication of a fully solution treated microstructure.

The safe-end material exhibits clearly delineated grain boundaries after the phosphoric etch, (See Figure 3-1). At some grain boundary locations, relatively large, discrete carbide particles are evident. Extensive matrix carbides are also resolved after the phosphoric acid etch. This

observed condition is consistent with the fact that the safe-end was subjected to two 1100^o-1175^oF stress relieving operations with a total time at temperature of approximately 16 hours.

The microstructure of the thermal sleeve is shown in Figure 3-2. It is evident from the features shown in these micrographs that the thermal sleeve is sensitized (carbides precipitated at grain boundaries). Apparently the material was furnished in the sensitized condition since no stress relief treatments were performed after installation of the thermal sleeve.

The grain size for the two components was determined to be:

Safe-end: ASTM 4.0-4.5

Thermal sleeve: ASTM 6.7

ASME SB 166 does not specify any limits for the grain size of wrought Inconel 600 material. However, the CB&I specification for nickel-chromium-iron forgings (MS-16) states that the grain size shall be as small as practical, with the objective of producing material with an ASTM grain size of 5.

CB&I specification MS-16 states that the Inconel forgings be furnished in the annealed condition in accordance with ASME SB 166. The ASME specification does not specify the particular heat treating parameters for the annealed condition, thus it is possible that material furnished to these specifications would be in a sensitized condition.

Micrographs illustrating the microstructure of the heat-affected-zones (HAZ) associated with the repair weld are shown in Figures 3-4 and 3-5. In each case, a zone of more pronounced grain boundary sensitization is apparent immediately adjacent to the fusion line. This feature is normal for the fabrication sequence employed, since sensitization in the HAZ is inherent in any welding of Inconel 600 and subsequent stress relieving would serve to enhance any earlier sensitization. The microstructure at locations 0.003 in. from the fusion line and beyond is comparable to that observed at locations remote from the weld [compare Figures 3-1(b) and 304]. The microstructural features within the HAZ are consistent with normal welding procedures and techniques.

The microstructure midway along the line of closest approach of the repair weld and the thermal sleeve attachment weld is shown in Figure 306(a). This structure is comparable to that at remote locations [compare with Figure 301(b)] indicating that the repair welding operation did not alter the microstructure in the vicinity of the thermal sleeve attachment.

The HAZ at the thermal sleeve attachment weld is shown in Figure 3-6(b). The microstructural features are similar to those of the repair weld HAZ and are normal for this situation. This zone was not involved in the cracking but the normal microstructure serves to indicate normal welding practice.

TABLE 3-1

CHEMICAL COMPOSITION

Item	Composition - Wt.%								
	Ni	Cr	Fe	Co	C	Mn	Cu	Si	S
Safe-end	74.82	15.18	8.61	0.06	0.07	0.18	0.13	0.29	0.005
Thermal Sleeve	77.42	14.86	6.98	0.04	0.07	0.28	0.01	0.15	0.005
ASME SB-166	72.0	14.0- 17.0	6.0- 10.0	Incl. w/Ni	0.15 Max.	1.00 Max.	0.50 Max.	0.50 Max.	0.015 Max.
Repair Weld	70.46	14.54	8.21	0.04	0.05	4.80	0.06	0.53	0.008
Attachment Weld	67.90	14.48	8.16	0.03	0.05	7.10	0.16	0.51	0.018
AWS-5.11-76 ENiCrFe-3	59.0 Min.	13.0 17.0	10.0 Max.	0.12 Max.	0.10 Max.	5.0- 9.5	0.5 Max.	1.0 Max.	0.015

FIGURE 3-1. MICROSTRUCTURE OF SAFE-END.
Location 1, Figure 3-3.

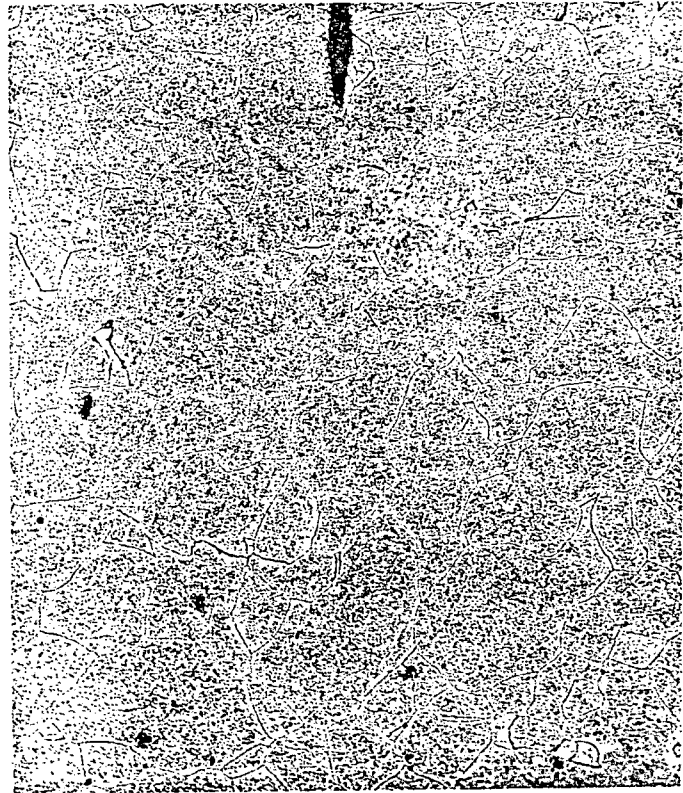
2-34432

100X

(b) 8:1 phosphoric acid electrolytic etch

2-34433

500X



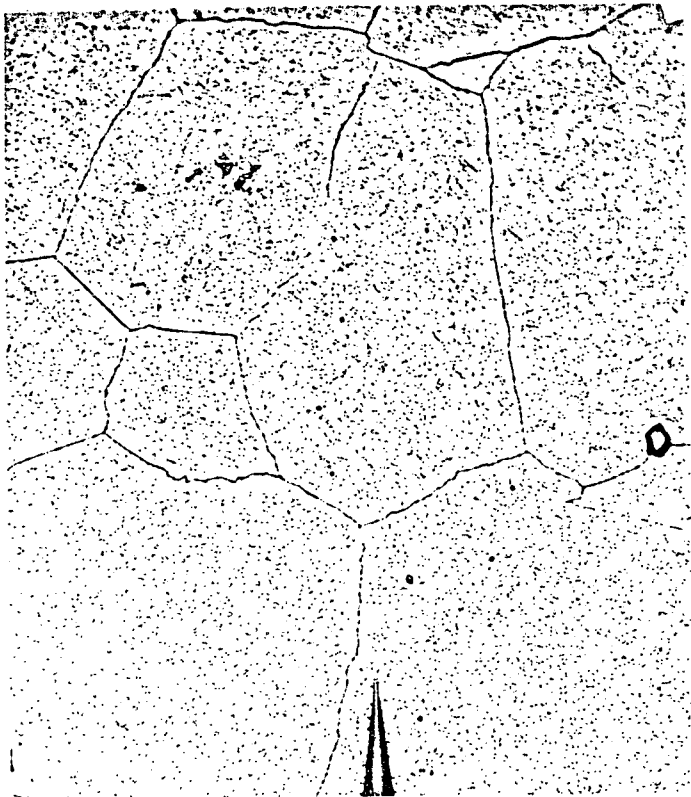
2-34400

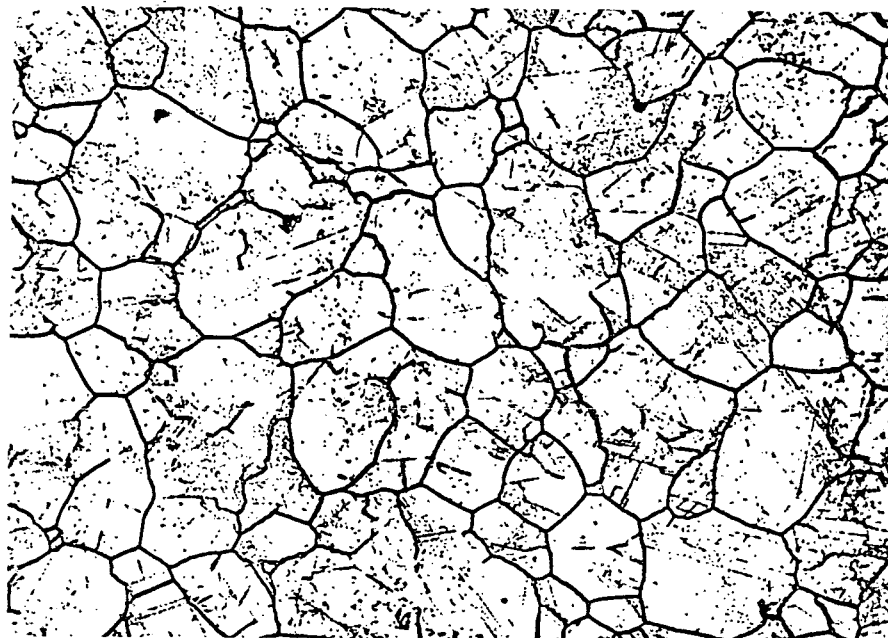
100X

(a) 10% electrolytic etch

2-34401

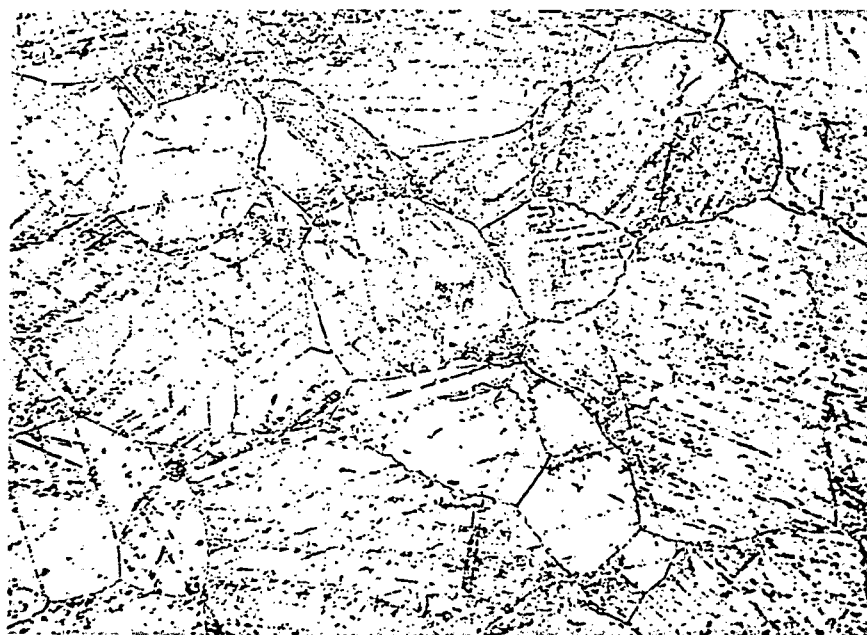
500X





2-34423

(a) 10% Nital etch. 200X



2-34486

(b) 8:1 Phosphoric acid etch. 500X

FIGURE 3-2. MICROSTRUCTURE OF THERMAL SLEEVE.
Location 2, Figure 3-3.

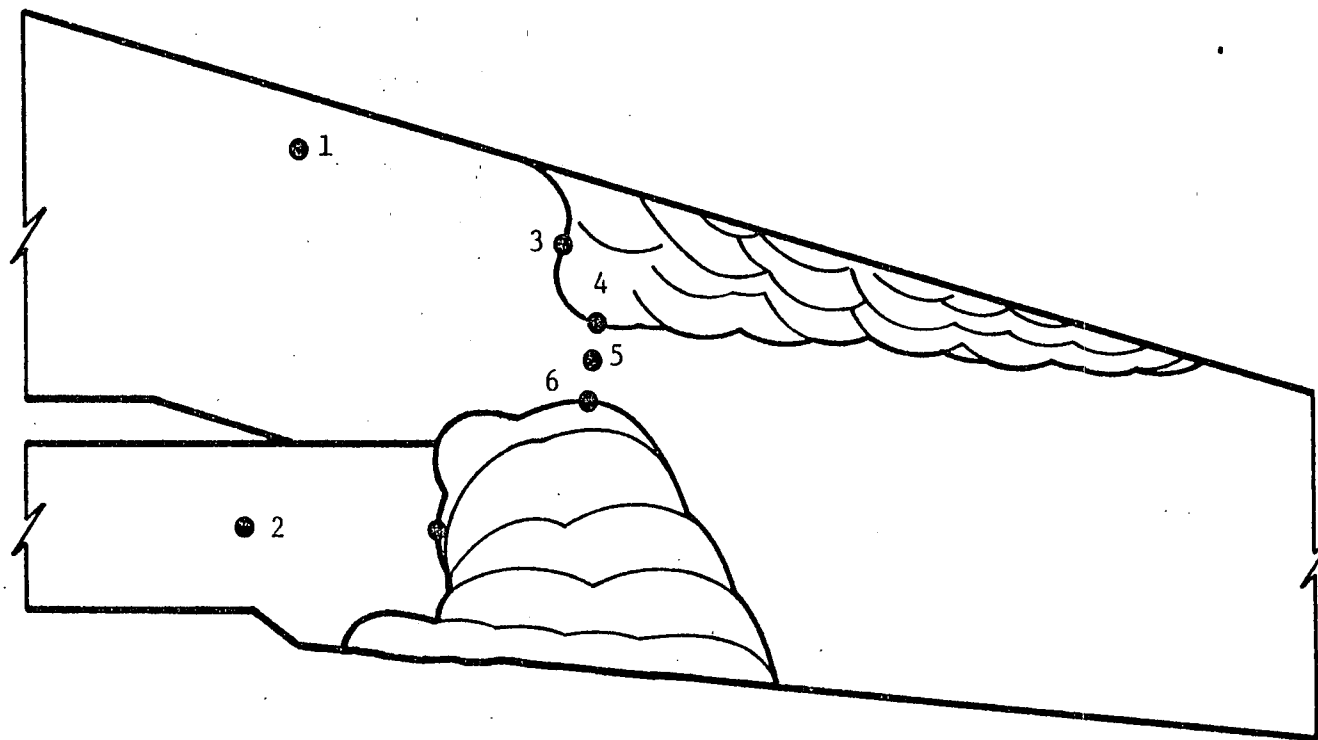
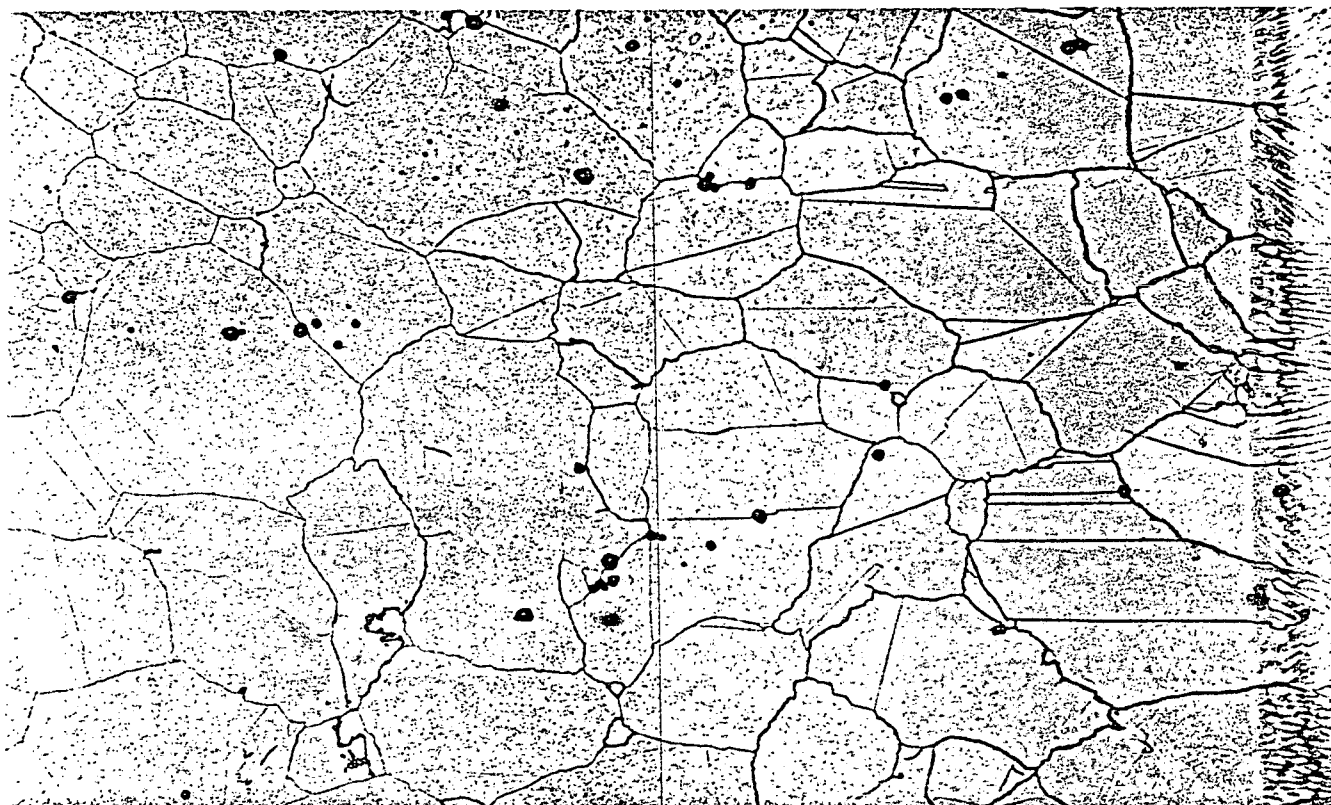


FIGURE 3-3. DIAGRAM OF REPRESENTATIVE SECTION THROUGH THERMAL SLEEVE ATTACHMENT AREA. 5X



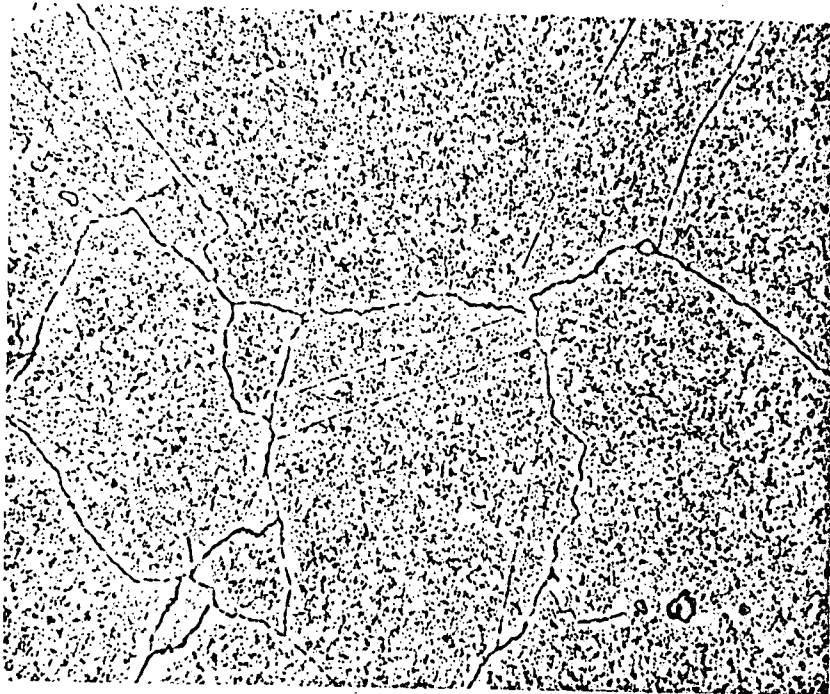
2-34398-399

FIGURE 3-4. MICROSTRUCTURE OF HAZ AT REPAIR WELD.
Location 3, Figure 3-3.
Etchant: 10% Nital, electrolytic. 200X



2-34396-397

FIGURE 3-5. MICROSTRUCTURE OF HAZ AT REPAIR WELD.
Location 4, Figure 3-3.
Etchant: 10% Nital, electrolytic. 200X



2-34431 500X
(a) Location 5. Phosphoric acid etch.

FIGURE 3-6. MICROSTRUCTURE OF HAZ AND BASE METAL
AT THERMAL SLEEVE ATTACHMENT WELD.
See Figure 3-3 for locations.



2-34394-395 200X
(b) Location 6. 10% Nital etch.

4.0 CHARACTERIZATION OF CRACKING

4.1 Microstructural Features

A critical metallographic examination of three sections (1-1, 4-4 and 5-5, Figure 1-4) through the thermal sleeve attachment area has been performed to establish the microstructural characteristics of the cracking. Micrographs illustrating particular features observed in these examinations are shown in Figures 4-1 through 4-7.

In each section the crack path was observed to be completely intergranular and crack initiation occurred within the HAZ of the root pass of the thermal sleeve attachment weld, see Figures 4-1, 4-4 and 4-6. The initial portion of the cracking followed a path parallel to the contour of the root pass fusion line. The cracks did not initiate exactly at the tip of the crevice where the highest stresses would be expected. This factor indicates that the weld metal is less susceptible than the base metal to the particular cracking mechanism.

In each section, a zone of re-solution treated material was observed adjacent to the fusion line of the root pass weld bead. In the metallographic sections, this zone appears as a lightly etched zone. A zone of more pronounced grain boundary sensitization is evident immediately beyond the re-solution treated zone.

In Section 1-1, crack initiation and early crack propagation occurred within the re-solution treated zones. The re-solution treated material adjacent to the crack path and the transition to the sensitized base metal structure are shown in Figures 4-2 and 4-3. In Section 4-4 the first portion of the crack path lies within the zone of material exhibiting the most pronounced sensitization (see Figure 4-4) while in Section 5-5 the crack path lies at the outer edge of the HAZ (Figures 4-6 and 4-7). These observations indicate that the degree of sensitization in the vicinity of the thermal sleeve attachment weld did not influence crack initiation or propagation.

Micrographs at the tip of the crack in Section 4-4 where the crack approaches the repair weld are shown in Figure 4-5. At this location, crack propagation has continued within unaffected base metal in spite of the proximity of the more heavily sensitized HAZ.

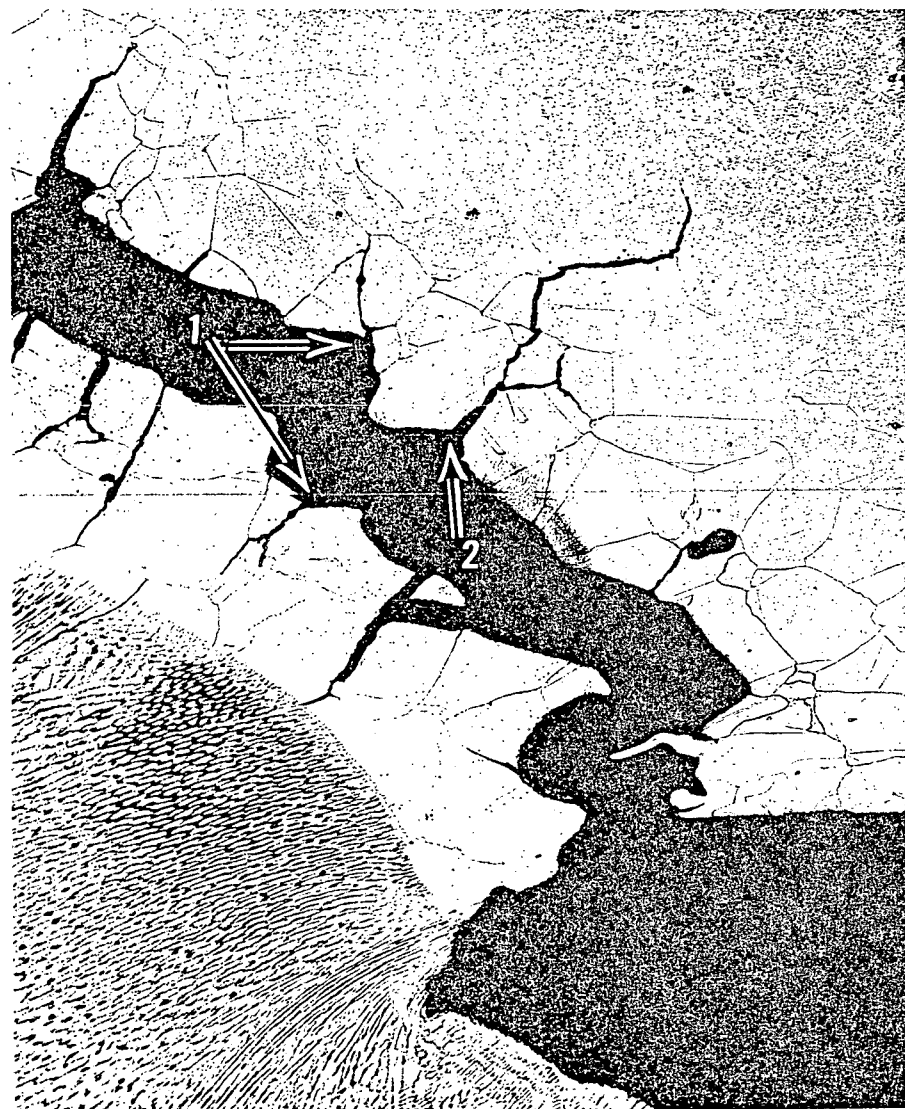
4.2 Fractographic Features

Two of the fractographic specimens (Nos. 1 and 4, Figure 1-4) have been examined in the scanning electron microscope (SEM). In general, very similar features were observed in each case. A macrograph of Specimen No. 1 is shown in Figure 4-8. SEM fractographs from that specimen illustrating the particular features observed to date are shown in Figures 4-9 through 4-13. Specimen No. 1 is from a location where the crack passed through the repair weld. A transition in surface topography marking the line of intersection of the crack with the repair weld is apparent in Figure 4-8. This particular specimen was decontaminated by light brushing and washing in a water/detergent solution prior to the SEM examination.

The fracture surface exhibited completely intergranular features at all locations examined. The intergranular nature of the fracture is evident in the lower magnification fractographs of Figures 4-9, 4-10 and 4-11. No evidence of any form of step-wise crack propagation was evident.

Some differences in the details of the intergranular facets were noted at various locations on the specimen. These differences are attributed to the surface condition and/or the presence of adherent deposits. At locations near the crack origin, individual facets exhibited fine-scale rounded features and surface deposits were not readily apparent, see Figure 4-9. Distinctly crystalline surface deposits were observed at locations a short distance from the inside edge as shown in Figure 4-10. At locations near the transition to weld metal fracture, other forms of surface deposit were noted as shown in Figures 4-11 and 4-12. In these cases, the deposit is clearly different from the crystalline deposits observed closer to the inside edge.

The typical topographic features of the zone of crack propagation in weld metal are shown in Figure 4-13. It is evident from these features that crack propagation in this zone occurred in an intercolumnar mode. The transition in surface topography at the intersection of the crack with the repair weld is strictly due to the characteristically different microstructures of the weld metal and base metal.



2-34434,-435

FIGURE 4-1. MICROSTRUCTURE AT TIP OF CREVICE. Section 1-1,
Figure 1-4, Etchant: 8:1 Phosphoric acid. 100X

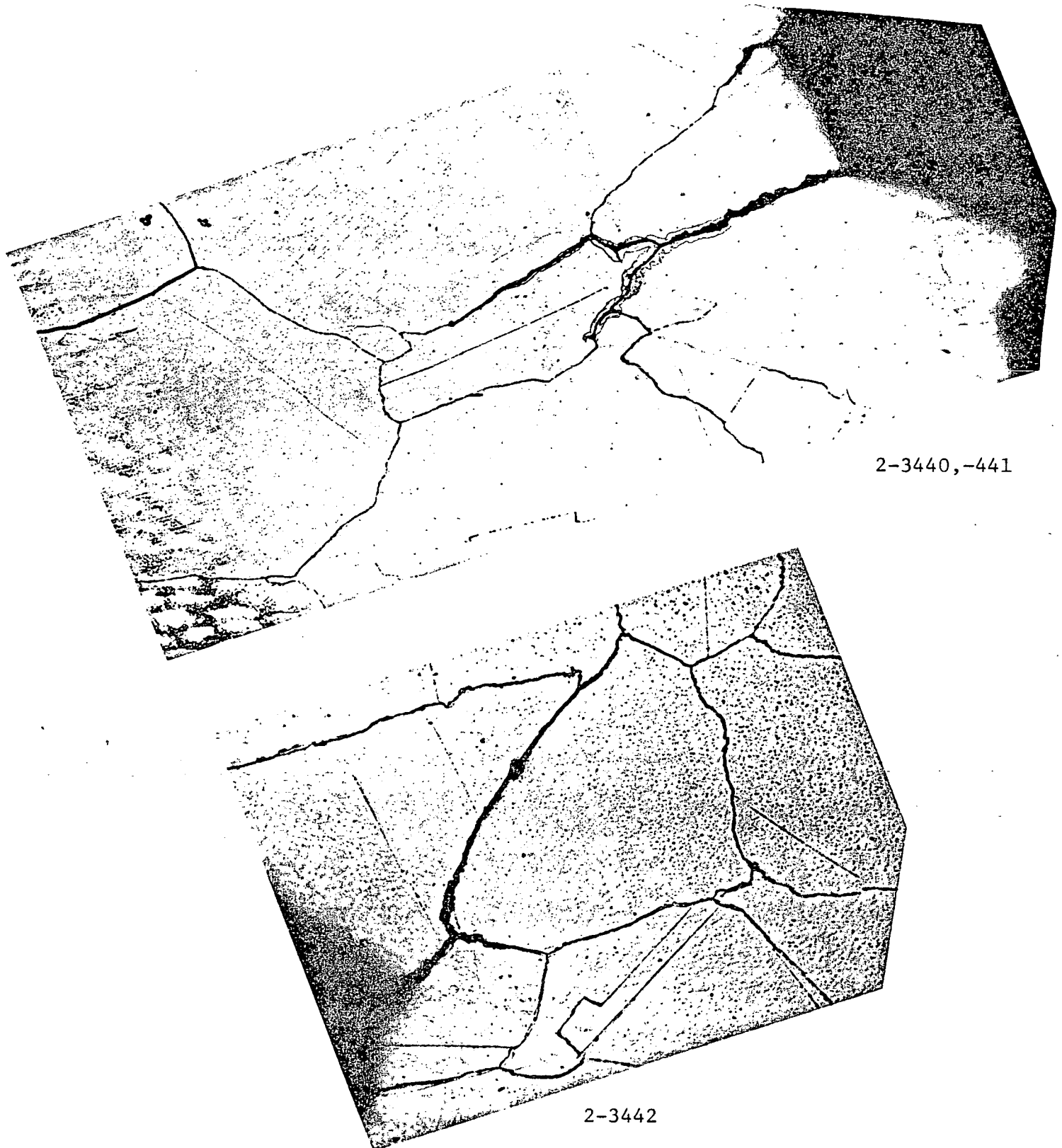
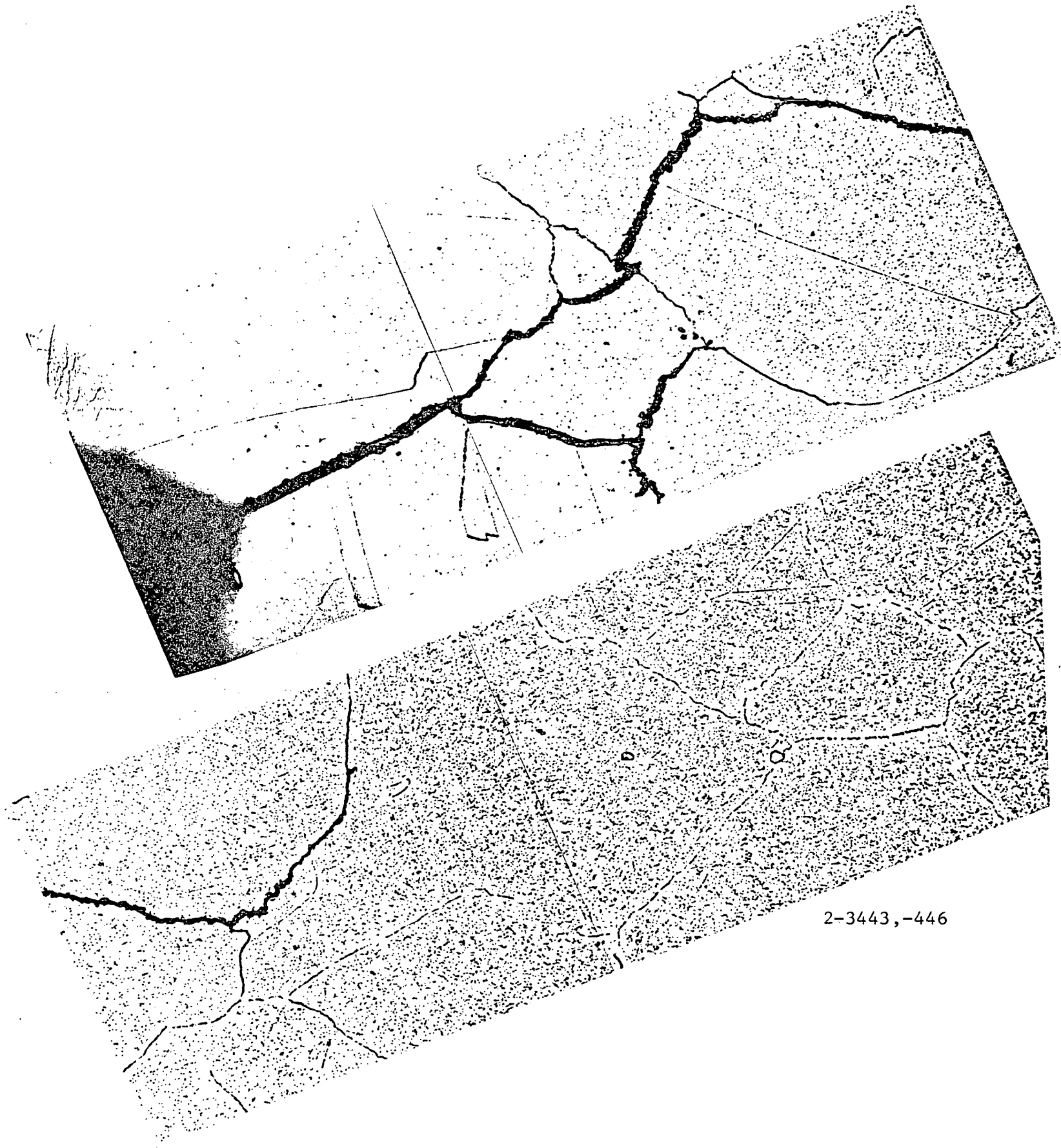
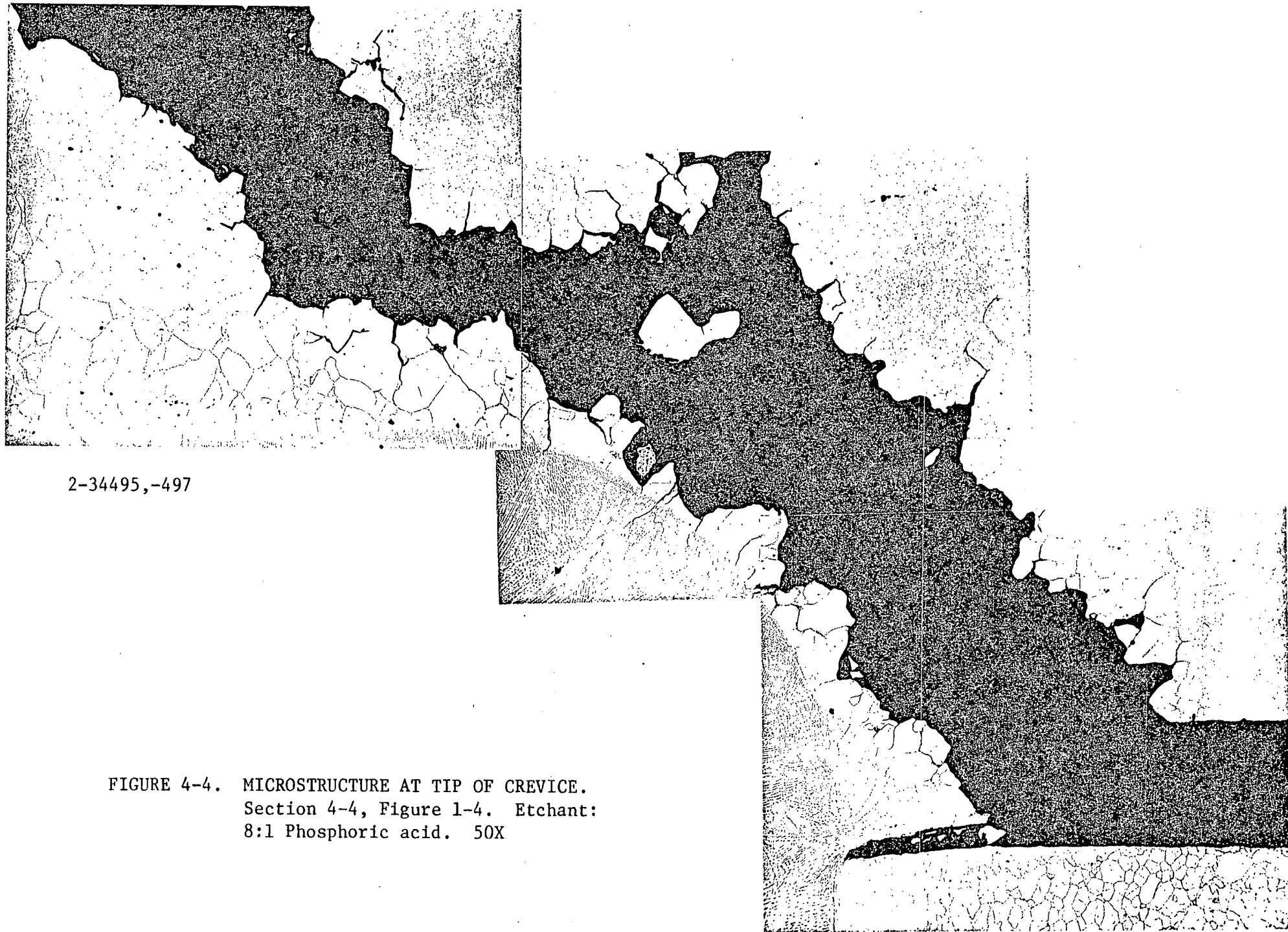


FIGURE 4-2. MICROSTRUCTURE AT POINTS ON OPPOSITE SIDES OF CRACK. Section 1-1, Location 1, Figure 4-1. Etchant: 8:1 Phosphoric acid. 500X



2-3443,-446

FIGURE 4-3. MICROSTRUCTURE AT MAIN CRACK. Section 1-1, Location 2, Figure 4-1. Arrows indicate match points. Etchant: 8:1 Phosphoric acid. 500X



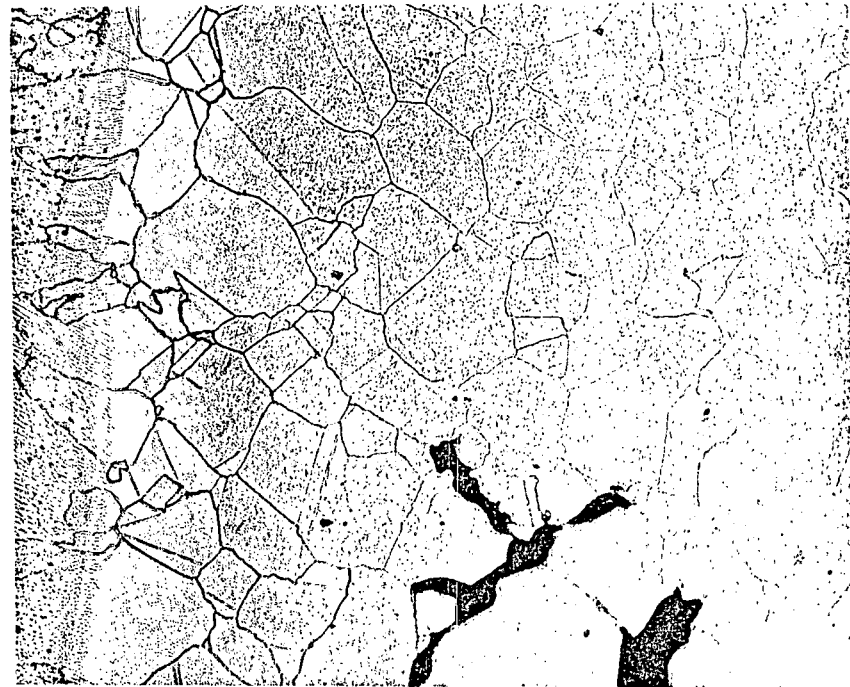
2-34495,-497

FIGURE 4-4. MICROSTRUCTURE AT TIP OF CREVICE.
Section 4-4, Figure 1-4. Etchant:
8:1 Phosphoric acid. 50X



2-34449

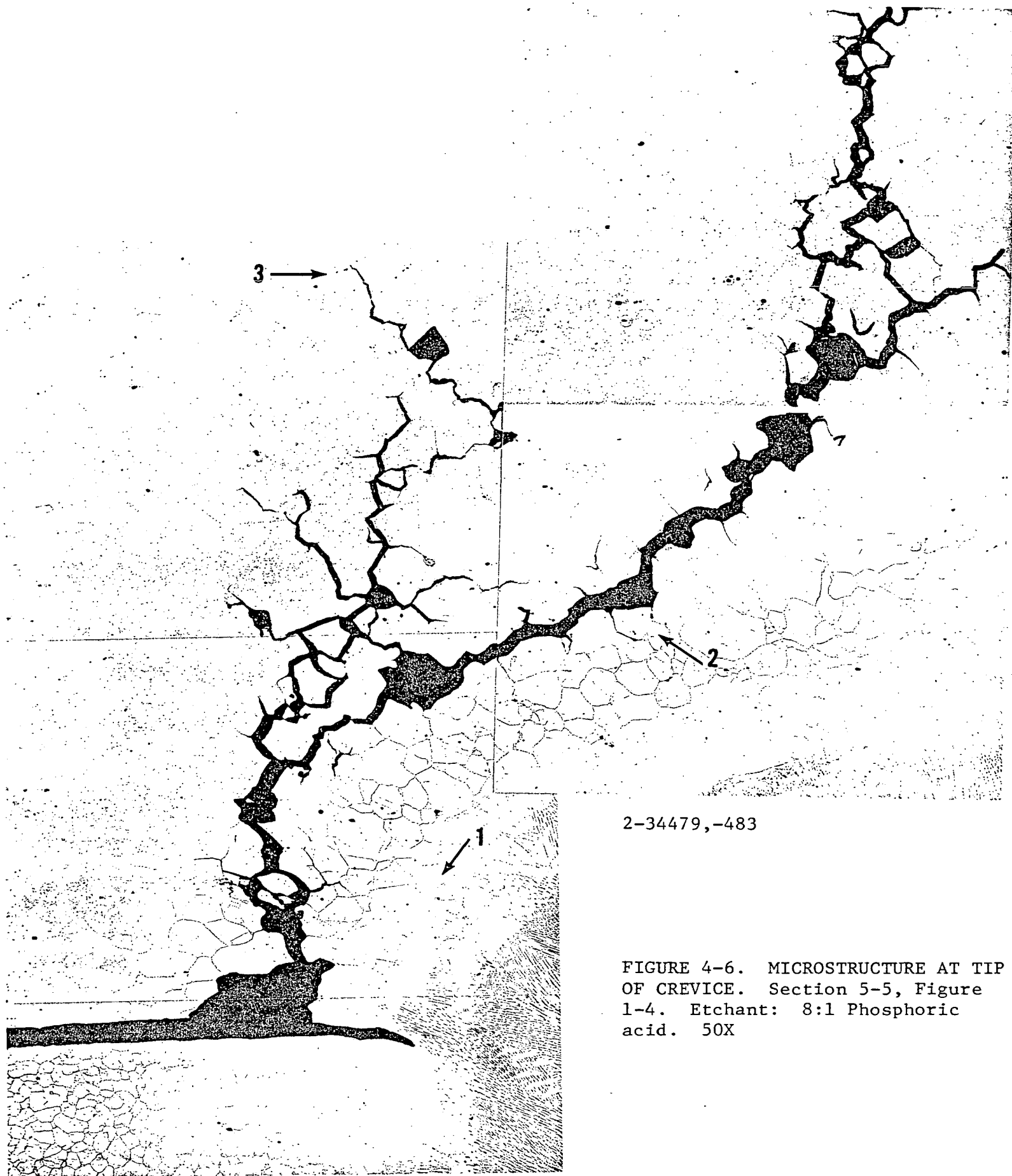
(a) 50X



2-34521

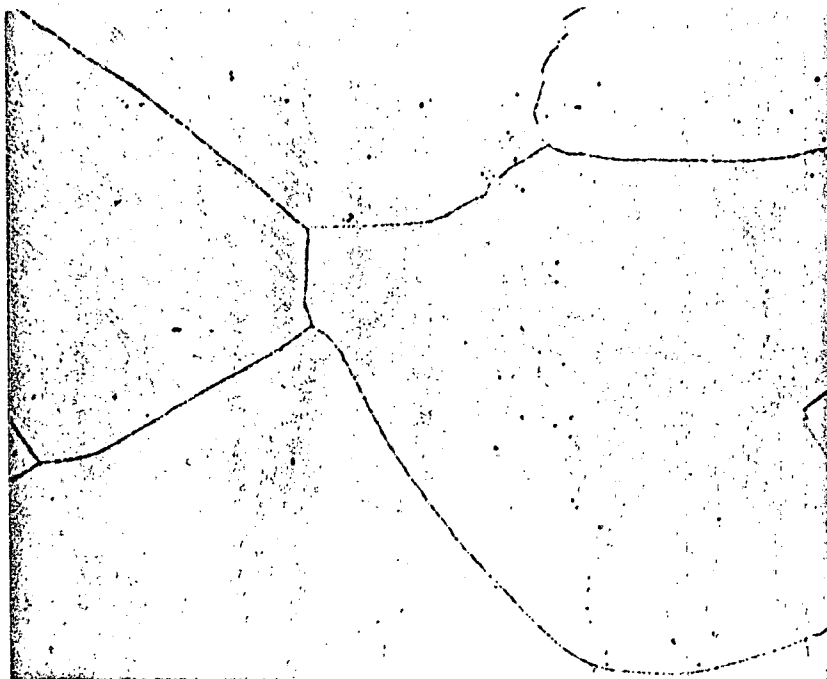
(b) 100X

FIGURE 4-5. MICROSTRUCTURE AT CRACK TIP. Section 4-4.
See Figures 2-3 and 4-4. Etchant: 8:1
Phosphoric acid.



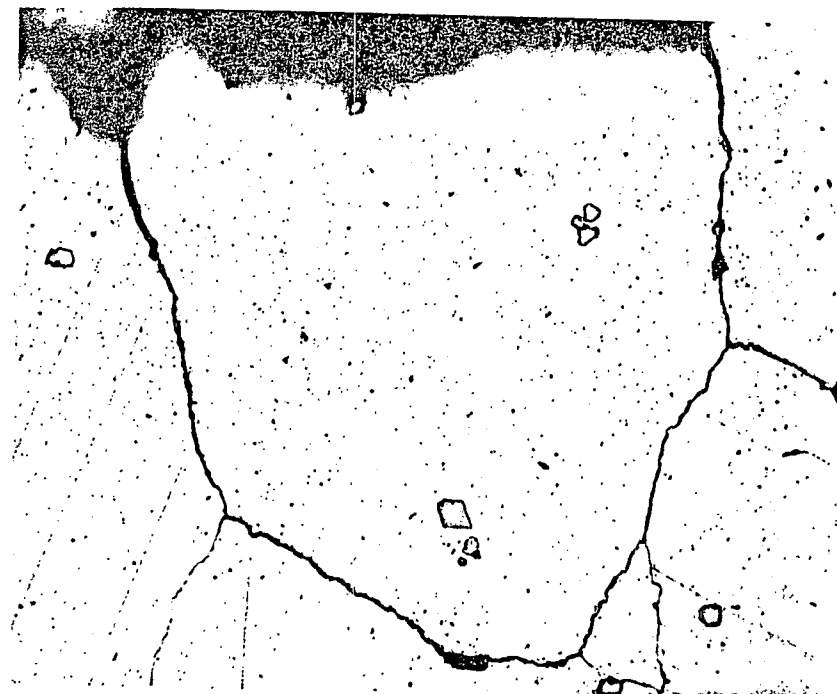
2-34479,-483

FIGURE 4-6. MICROSTRUCTURE AT TIP OF CREVICE. Section 5-5, Figure 1-4. Etchant: 8:1 Phosphoric acid. 50X



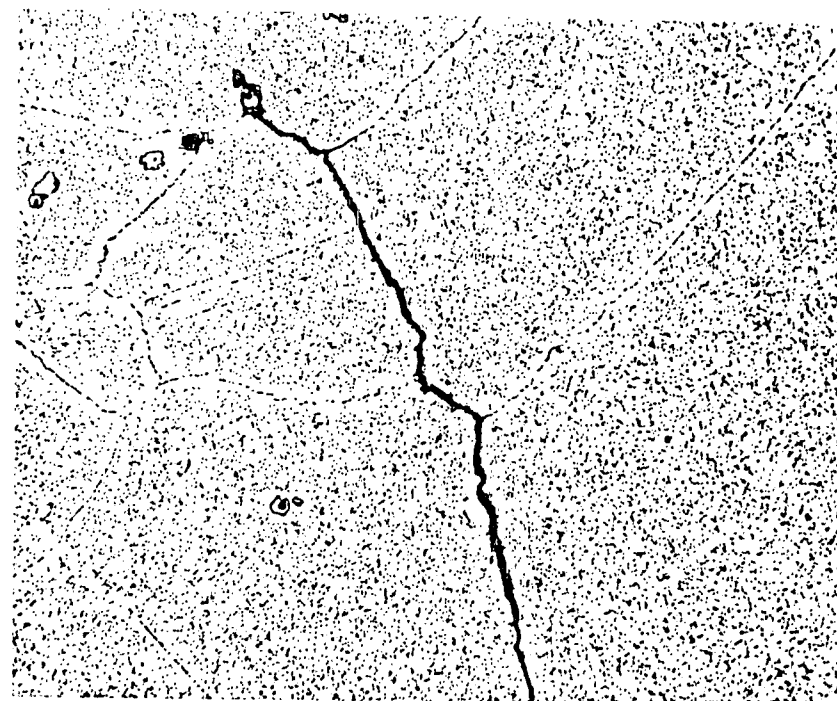
2-34488

(a) Re-solution treated zone. Location 1.



2-34484

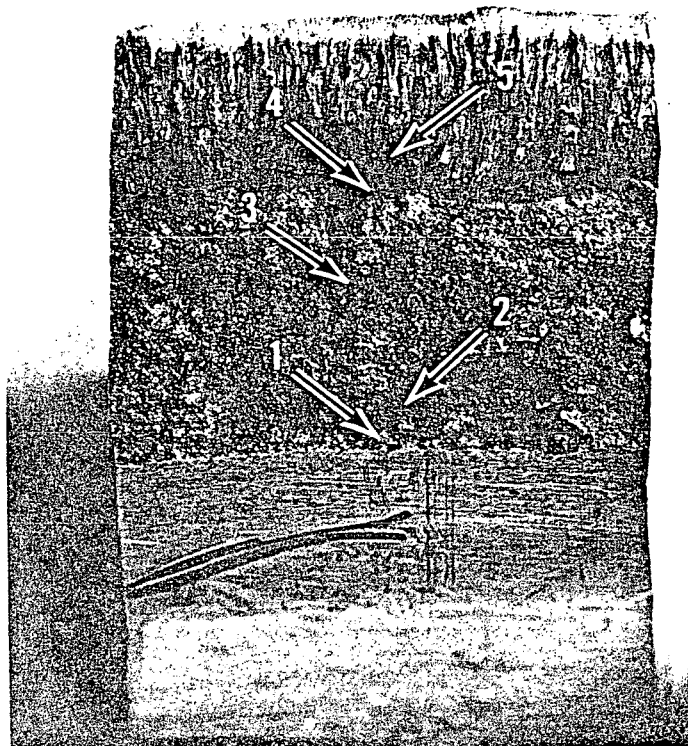
(b) At main crack.



2-34485

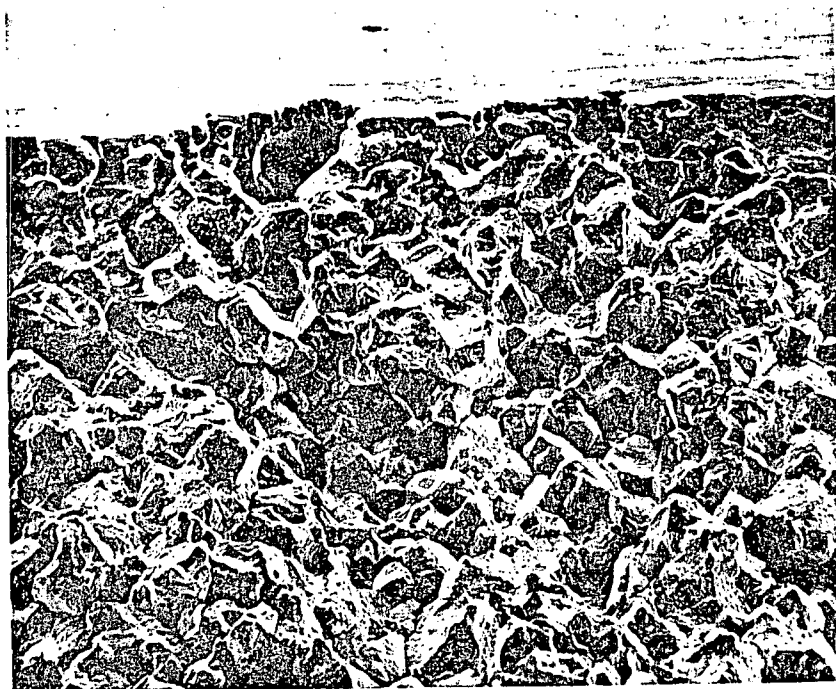
(c) At crack tip.

FIGURE 4-7. MICROSTRUCTURE IN VICINITY OF MAIN CRACK. Section 5-5, See Figure 4-6 for locations. Etchant: 8:1 Phosphoric acid. 500X



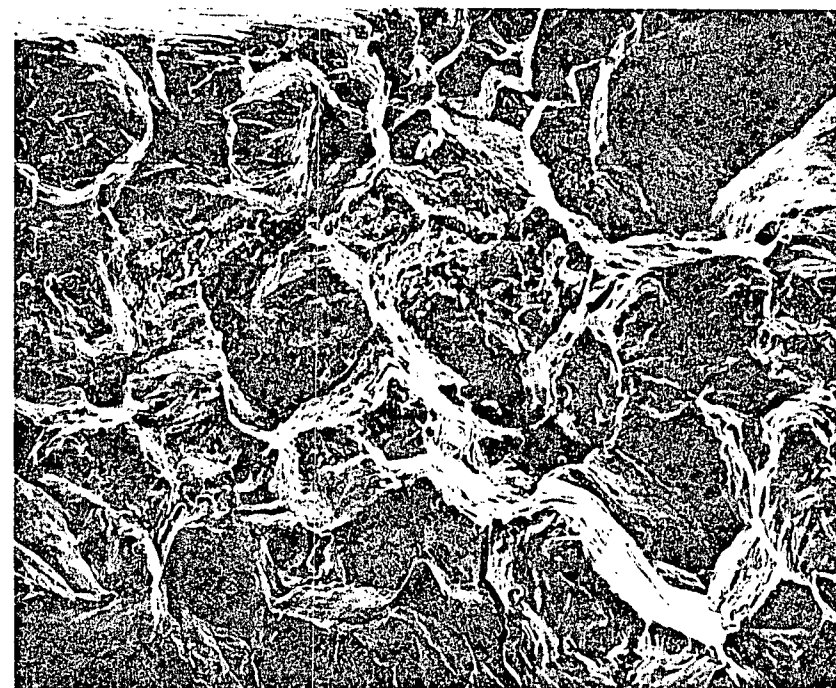
2-34351

FIGURE 4-8. CRACK SURFACE SPECIMEN. Specimen No. 1,
Figure 1-4. 3X



2-1145

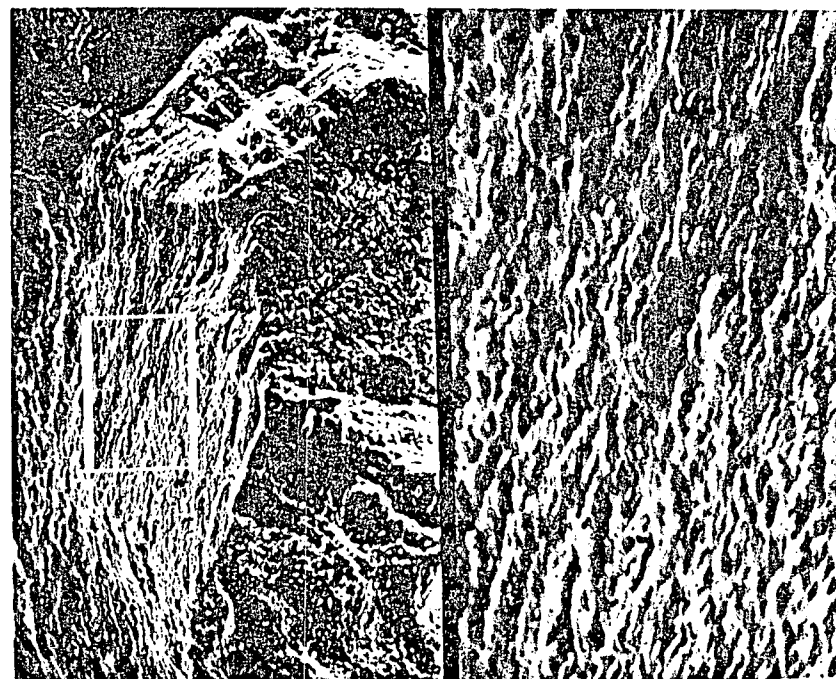
50X



2-1155

150X

FIGURE 4-9. SEM FRACTOGRAPHS FROM CRACK SURFACE.
Specimen No. 1, Location 1, Figure 4-8.



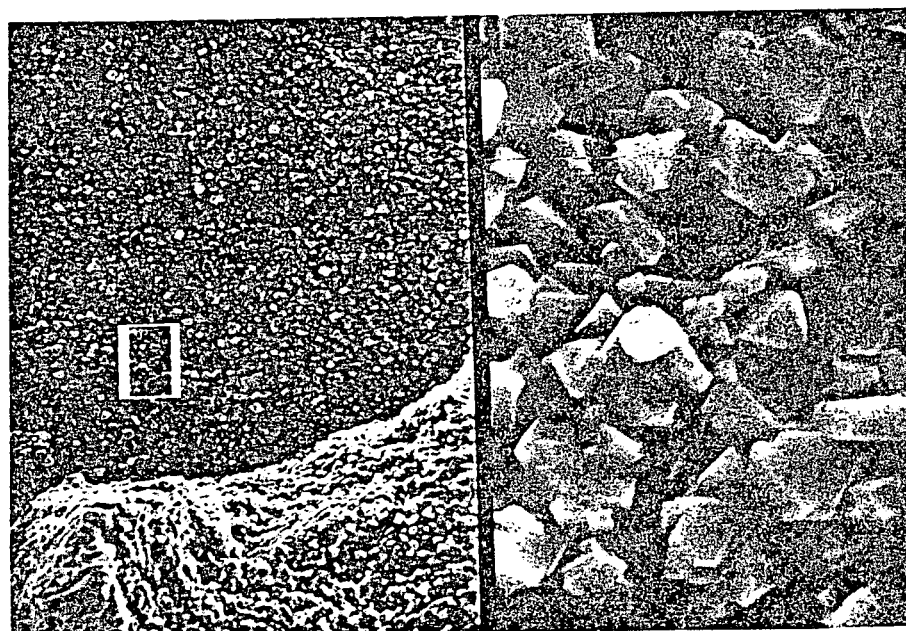
2-1735

1000/5000X



2-1175

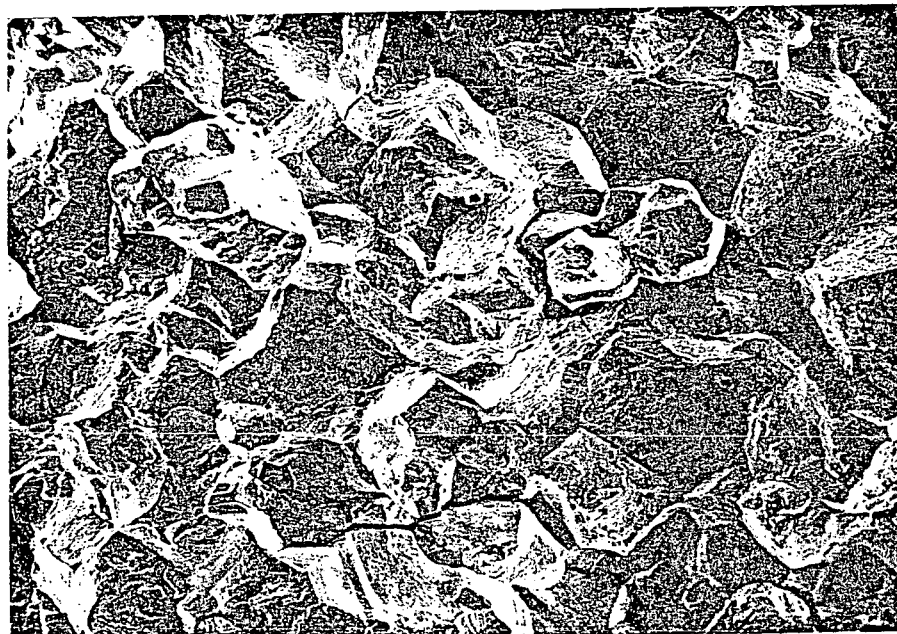
150X



2-1785

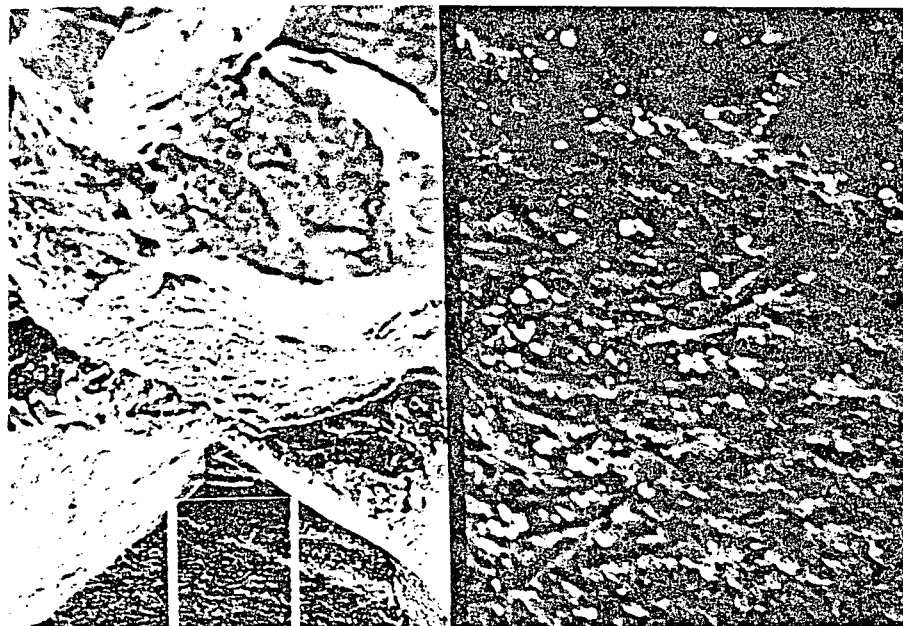
1000/10,000 X

FIGURE 4-10. SEM FRACTOGRAPHS FROM CRACK SURFACE.
Specimen No. 1, Location 2, Figure 4-8.



2-1795

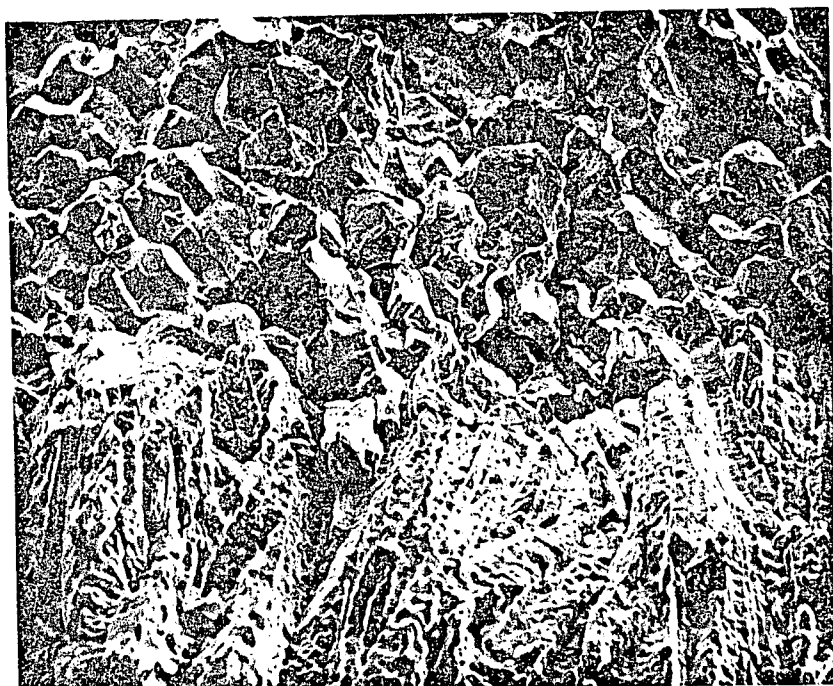
100X



2-1823

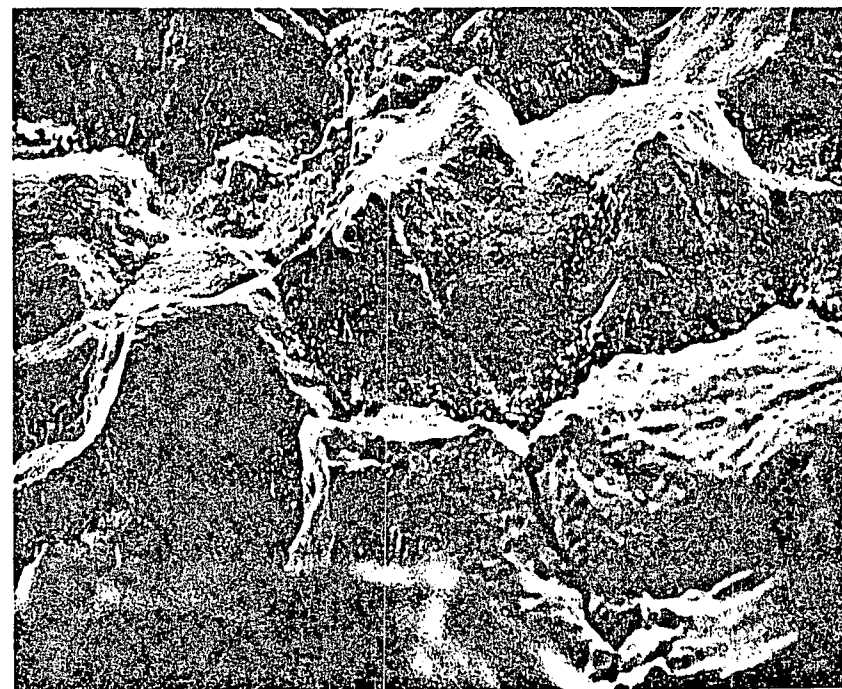
500/2000

FIGURE 4-11. SEM FRACTOGRAPHS FROM CRACK SURFACE.
Specimen No. 1, Location 3, Figure 4-8.



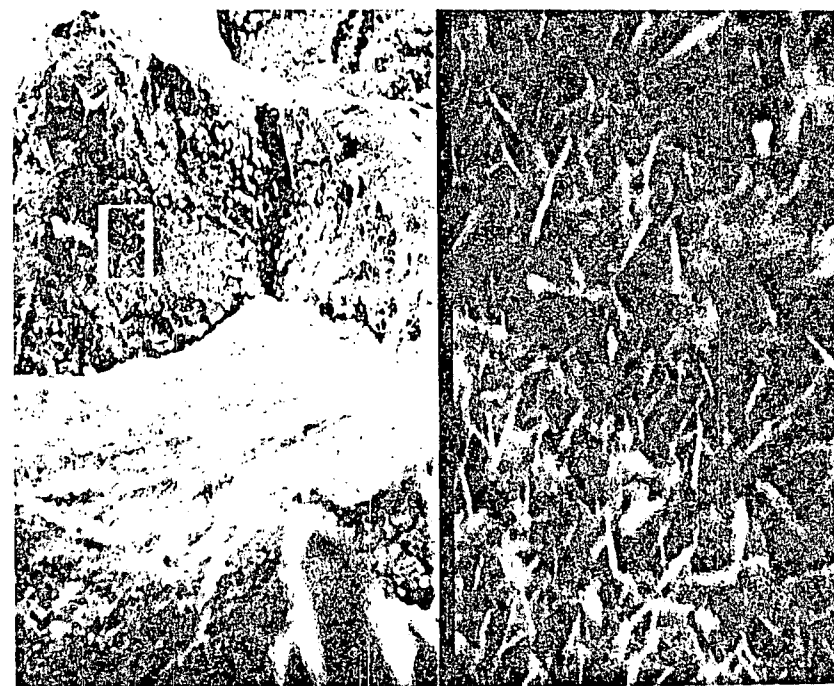
2-1195

50X



2-1865

300X



2-1905

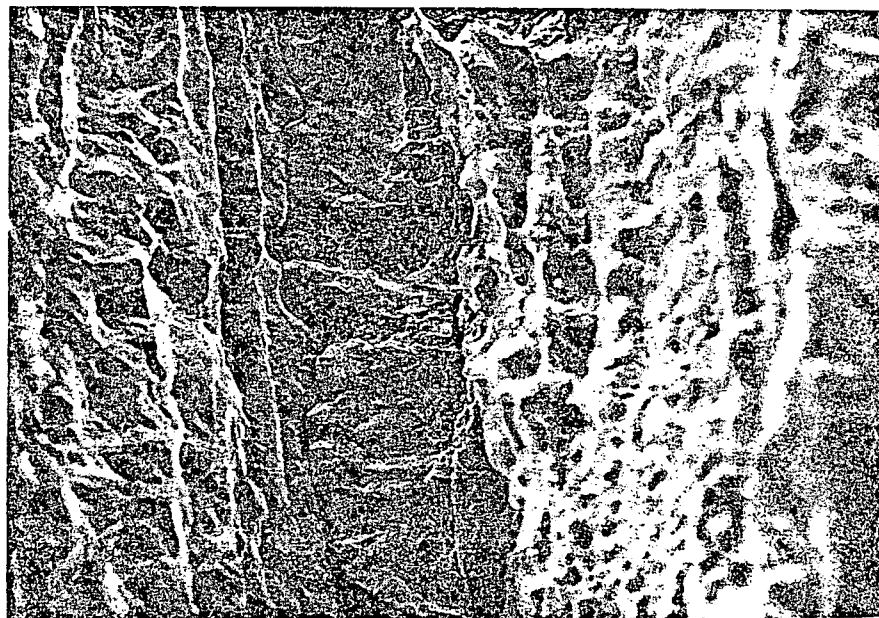
500/5000X

FIGURE 4-12. SEM FRACTOGRAPHS FROM CRACK SURFACE.
Specimen No. 1, Location 4, Figure 4-8.



2-1915

50X



2-1925

300X

FIGURE 4-13. SEM FRACTOGRAPHS FROM CRACK SURFACE.
Specimen No. 1, Location 5, Figure 4-8.

5.0 SURFACE DEPOSIT ANALYSES

Energy dispersive X-ray (EDS) analytical techniques have been employed in the examination of two crack surface specimens (Nos. 5 and 6, Figure 1-4) to provide in situ qualitative analyses of surface deposits. These particular specimens were not cleaned and particular care was exercised in cutting and handling to prevent extraneous contamination and preserve the surface deposits.* The data obtained to date from these examinations are summarized as follows:

1. Definite evidence of the presence of sulfur on the fracture surfaces of both specimens was obtained.
2. The magnitude of the sulfur indications was significantly higher at points near the end of the crack than at points near the origin.
3. At each point examined, the sulfur was distributed evenly over the surface.
4. Locations on the crevice surface adjacent to the inside edge of the crack surface did not exhibit any evidence of sulfur.
5. Iron was identified as the only other principal constituent (detectable by EDS) present in the surface deposits.
6. No other extraneous contaminant species have been detected.

Further laboratory work to extend the surface deposit evaluation is in progress.

*The analyses were performed at the Argonne National Laboratory where facilities for SEM examination of radioactively contaminated materials are available.

6.0 SUMMARY AND CONCLUSIONS

The observations made to date in this investigation may be summarized as follows.

1. Significant cracking occurred on the inside surface of the safe-end over a full 360° of circumference.
2. All cracking initiated in the immediate vicinity of the tip of the tight crevice between the thermal sleeve and the safe-end.
3. Crack initiation was confined to a single location on the crevice surface at any one angular position.
4. No incipient intergranular attack, pitting or other evidence of significant chemical attack of the safe-end was present along the surface of the tight crevice.
5. Cracking occurred completely within the safe-end forging, except for the later stages at some locations, where the crack propagated through the repair weld.
6. Crack initiation and the early stage of crack propagation occurred both in a re-resolution treated zone and in the sensitized zones adjacent to the root-pass of the thermal sleeve attachment weld.
7. The cracking was completely intergranular at all locations examined, including both the initiation and the propagation stages.
8. No evidence of any step-wise crack propagation has been observed to date. Also, there are no fractographic features to indicate discrete initiation sites around the periphery of the crack.
9. Significant amounts of sulfur have been detected in the deposits on the crack surfaces of two specimens from the safe-end, but the type of sulfur species (i.e., $\text{SO}_4^{=}$, S, $\text{S}^{=}$, etc.) has not been identified. Sulfur was not detected on the tight crevice surfaces of the particular specimens examined. No evidence of any other extraneous contaminant species has been observed on the crack surface or crevice surface.
10. Both the safe-end material and the thermal sleeve material are in a sensitized condition. This condition is considered normal for this particular case in view of the post-weld stress relieving

treatment, applicable specifications, and usual mill practice.

11. The chemical composition of the safe-end material and the thermal sleeve material conform to ASME Specification SB 166.
12. The weld deposit chemistry for both welds conforms to AWS-5.11-76.
13. The repair welding operation on the outside of the safe-end did not result in any modification of the microstructure in the vicinity of crack initiation.

The metallographic and fractographic characteristics of the cracking (completely intergranular with no significant direct corrosive attack) serve to identify the cracking mechanism as intergranular stress corrosion cracking (IGSCC). Numerous laboratory studies have shown Inconel 600 to be susceptible to such cracking in high-purity water environments in certain circumstances (1-3)*. In this published data, incubation times are long, often greater than one year, and no cracking has been observed at stress levels below the yield strength.

A pertinent factor indicated by data in the literature is that the metallurgical condition of Inconel 600 (i.e., sensitized vs solution annealed) does not have a critical influence on susceptibility to IGSCC (2-6). This particular factor is evident in the observations made in this investigation in that cracking was observed to occur both in re-solution treated material and in sensitized material adjacent to the attachment weld. In view of this factor, and the fact that no other microstructural abnormalities were apparent, the observed sensitized condition of the safe-end cannot be considered as a contributing factor to the cracking problem.

In many materials/environment combinations the presence of a tight crevice can result in severe localized corrosive attack or stress-corrosion cracking. Thus, attention must be directed to the possible role of the tight crevice in IGSCC of Inconel 600 in reactor water environments. It is not likely that the classical differential aeration cell would develop at a crevice in a uniform high-purity water environment, but such regions could entrap air during outages, causing locally high oxygen levels on start-up. Also, if any anionic contaminant is present, acidification of the crevice could develop. Such a condition is known to enhance the susceptibility of Inconel 600 to IGSCC (5, 7). It has been demonstrated that the presence of a crevice significantly

*References listed on page 44.

accelerates cracking in low pH and high oxygen content solutions (5, 7), suggesting that a similar effect may occur in higher purity water environments. In view of these factors, it is likely that the presence of the crevice is a principal contributing factor to the present cracking problem.

No correlation between the presence of sulfur on the crack surfaces and cracking process can be made at this time. Also, the source and form of the sulfur has not been identified. To date it has not been established whether the sulfur detected on the crack surface is associated with the bulk composition of the safe-end or whether it is the result of progressive concentration of a contaminant species within the crevice.* If a sulfur species was entrapped from the environment it could lead to acidification of the crevice and contribute to cracking as discussed above. Further investigation of the nature and distribution of surface deposits is necessary to evaluate the observations made to date.

Consideration must be given to the source of stresses necessary to IGSCC. It is evident that stresses in the vicinity of the tip of the crevice are the result of applied stresses associated with service loading and residual stresses associated with the welds. It is likely that such stresses would not be uniform around the circumference of the safe-end. Therefore, any cracking controlled by such applied stresses would be expected to be biased toward one location. Also it is important to note that cracking developed through more than 50% of the cross sectional area of the safe-end and unstable fracture did not result. Subsequent metallographic and fractographic examinations did not reveal any significant plastic deformation at the tip of the part-through crack. These factors demonstrate that any axial stress component at the crack location, associated with in-service loading, is relatively low.

It is generally recognized that typical butt welds result in tensile residual stresses on the order of the yield strength of the material. Therefore, residual stresses of this magnitude must be considered to exist at the thermal

*In some laboratory investigations, significant amounts of sulfur have been observed on intergranular fracture surfaces for Inconel 600 specimens tested in very high purity water (2). This effect was attributed to sulfur segregation at grain boundaries in the initial microstructure.

sleeve attachment weld. Such stresses would be relatively uniform around the circumference of the crevice tip. In view of the fact that cracking occurred completely around the inside surface and of the relatively uniform extent of cracking, it is likely that residual stresses associated with the thermal sleeve attachment weld are the principal driving force for cracking.

The fact that no multiple cracking occurred along the crevice is significant. The distribution of residual stress near a butt weld is such that tensile stresses in the order of the yield strength exist in the immediate vicinity of the fusion line. The magnitude of the tensile residual stress decreases with distance from the fusion line. Therefore, the fact that crack initiation occurred only at one point near the weld indicates that relatively high stresses are necessary to induce cracking of Inconel 600 in these particular service conditions.

The existence of significant residual stresses in the crack initiation zone due to the repair weld has not been demonstrated. However, consideration of general principles concerning residual stresses developed from welding operations, indicate that the repair weld would have resulted in compressive hoop stresses and compressive axial stresses at the thermal sleeve attachment location which would not favor SCC. Regardless of the nature of the initial residual stresses associated with the repair weld, such stresses would be altered by subsequent machining and welding. The welding operation performed to attach the thermal sleeve would completely relieve all pre-existing stresses in the vicinity of the crevice tip. Therefore, the final state of stress at the location of eventual crack initiation would be completely controlled by the thermal sleeve attachment weld. In view of these factors, it is not likely that residual stresses from the weld repair contributed to crack initiation or the early stages of propagation.

In view of the factors discussed above, the information and data obtained to date this investigation support the following conclusions:

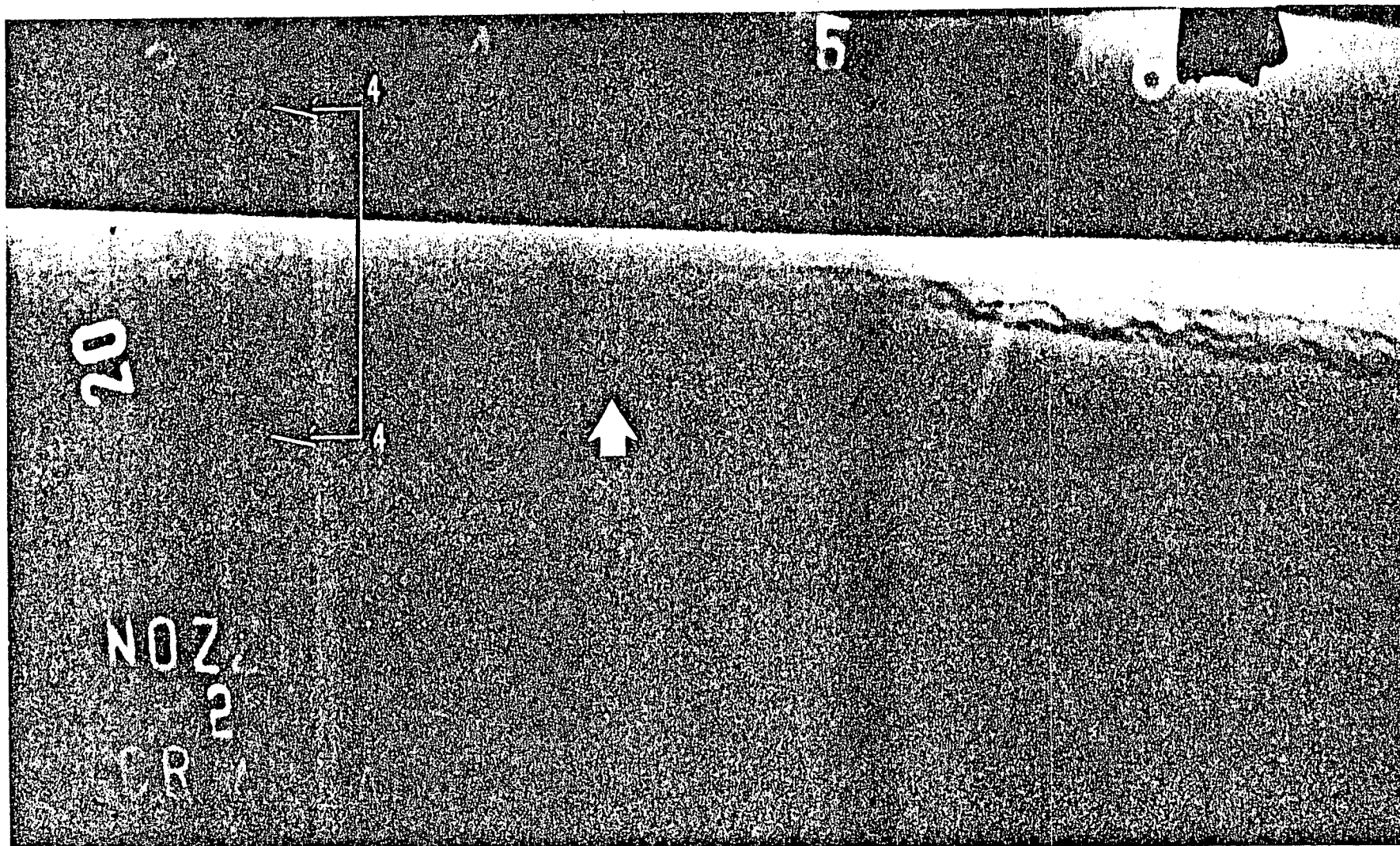
1. The cracking and eventual leakage encountered in the safe-end occurred by intergranular, stress corrosion cracking under the combined influence of residual stresses associated with the thermal sleeve attachment weld and environmental conditions associated with the tight crevice between the thermal sleeve and the safe-end.

2. The presence of sulfur on the crack surfaces suggests a possibility that a contaminant species could have contributed to crack initiation and propagation. This factor has not been completely resolved to date, but a contaminant species is neither a necessary or sufficient condition for cracking.
3. The sensitized condition of the safe-end material is not a contributing factor to the cracking problem.
4. There is no evidence to indicate that the existence of the repair weld on the outside of the safe-end contributed to crack initiation or the early stages of crack propagation.

REFERENCES

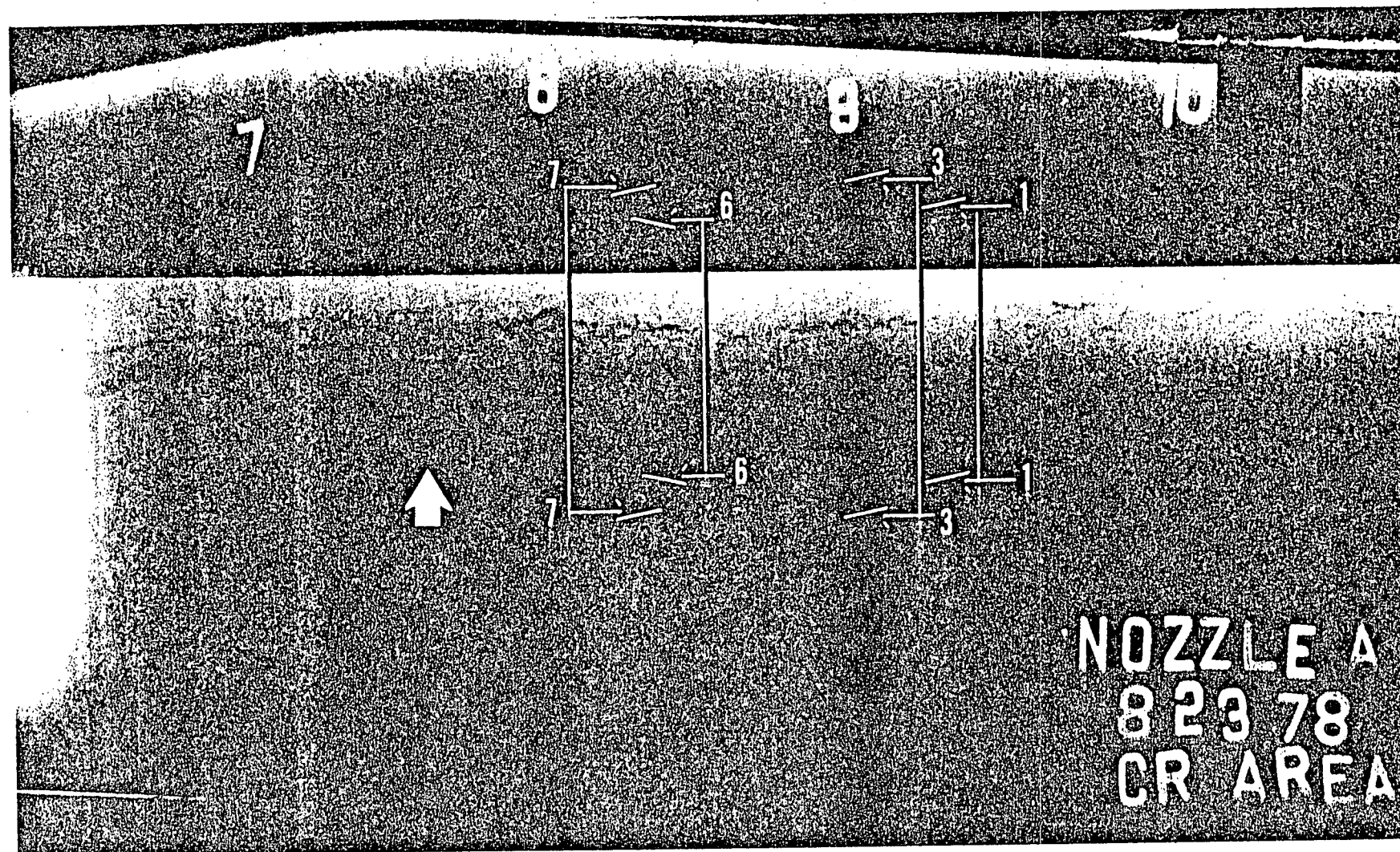
1. R. L. Cowan, II and C. M. Gordon, "Stress-Corrosion Cracking and Hydrogen Embrittlement of Iron-Base Alloys," p 1023, NACE, Houston (1977).
2. J. Blanchet, H. Coriou, L. Grall, C. Mahieu, C. Otter and G. Turbuer, "Stress-Corrosion Cracking and Hydrogen Embrittlement of Iron-Base Alloys," p 1149, NACE, Houston (1977).
3. H. A. Damian, R. H. Emanuelson, L. W. Sarver, G. J. Theus and L. Katz, Corrosion, 33, p 26 (1977).
4. H. Coriou, L. Grall, P. Olivier and H. Willermoz, "Fundamental Aspects of Stress-Corrosion Cracking," p 352, NACE, Houston (1969).
5. H. R. Copson and G. Economy, Corrosion, 26, 55 (1968).
6. F. W. Pement and N. A. Graham, "Corrosion Problems in Energy Conversion and Generation," The Electrochemical Society, Inc., Princeton (1974).
7. H. R. Copson and S. W. Dean, Corrosion, 21, p 1 (1965).

APPENDIX A
RADIOGRAPHS



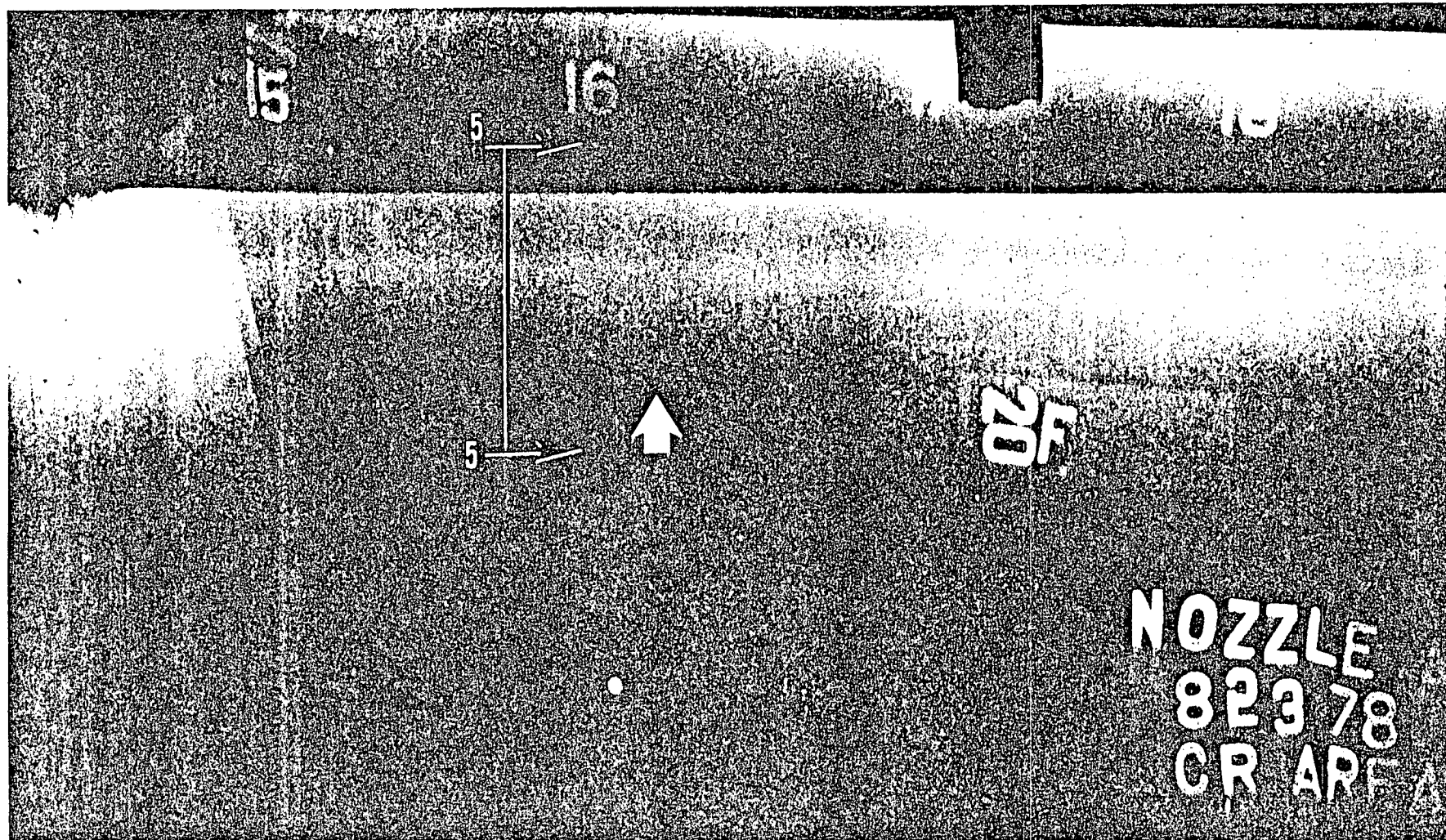
2-34468

FIGURE A-1. SAFE-END RADIOGRAPH. Stations 3 to 6. See Figure 1-4 for location. Section markers indicate location of metallographic sections. Block arrow indicates direction toward vessel.



2-34466

FIGURE A-2. SAFE-END RADIOGRAPH. Stations 7 to 10. See Figure 1-4 for location. Section markers indicate location of metallographic sections. Block arrow indicates direction toward vessel.

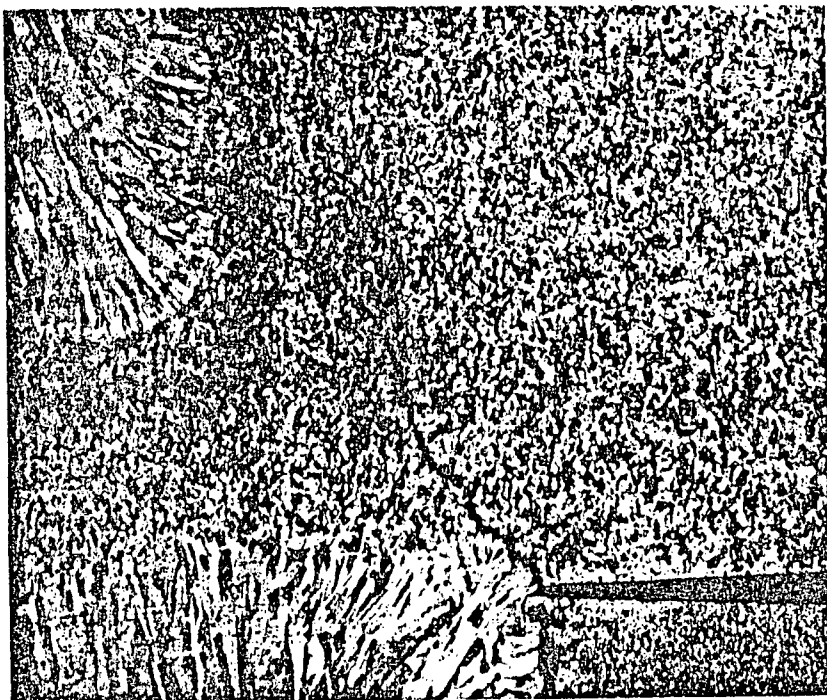


2-34467

FIGURE A-3. SAFE-END RADIOGRAPH. Stations 15 to 18. See Figure 1-4 for location. Section markers indicate location of metallographic sections. Block arrow indicates direction toward vessel.

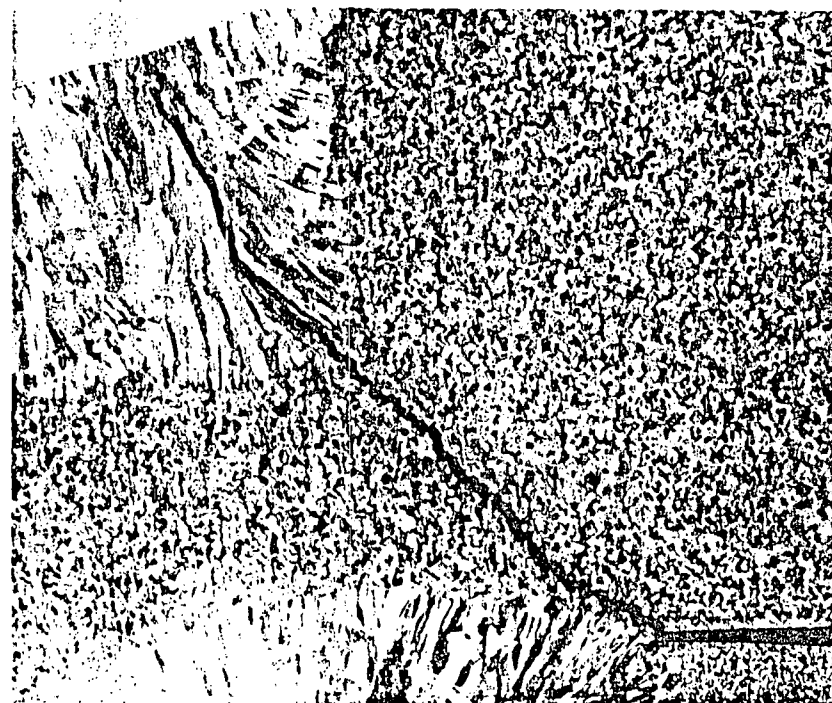
APPENDIX B

MACROGRAPHS OF METALLOGRAPHIC SECTIONS



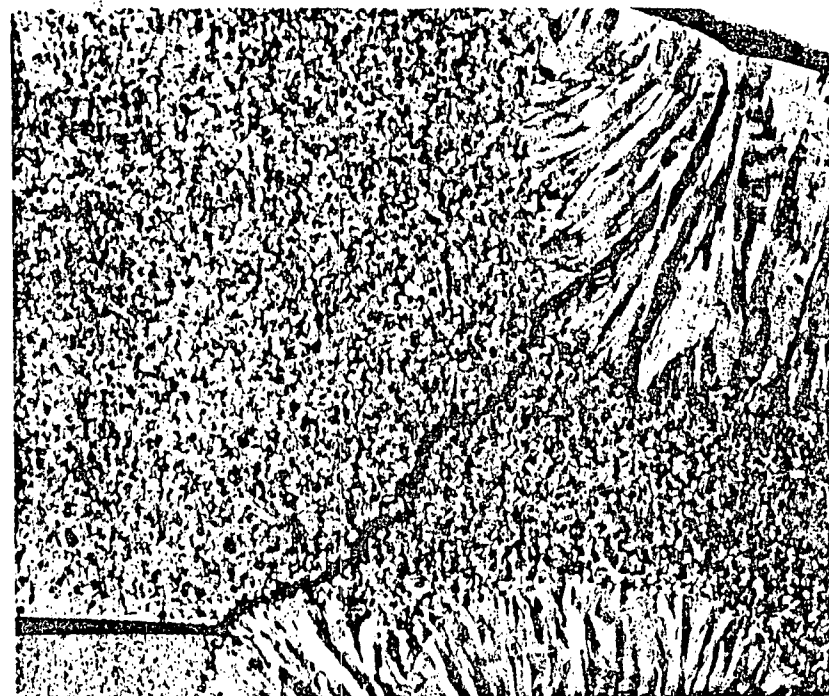
2-34350

(a) Section 3-3



2-34464

(b) Section 6-6



2-34465

(c) Section 7-7

FIGURE B-1. LONGITUDINAL SECTIONS AT THERMAL SLEEVE ATTACHMENT. See Figure 1-4 for locations. Lapito's etch. 5X